

ASSESSING SPATIAL DISPARITIES: A BAYESIAN LINEAR REGRESSION APPROACH

KYLE LIN WU AND SUDIPTO BANERJEE

ABSTRACT. Epidemiological investigations of regionally aggregated spatial data often involve detecting spatial health disparities between neighboring regions on a map of disease mortality or incidence rates. Analyzing such data introduces spatial dependence among the health outcomes and seeks to report statistically significant spatial disparities by delineating boundaries that separate neighboring regions with widely disparate health outcomes. However, current statistical methods are often inadequate for appropriately defining what constitutes a spatial disparity and for constructing rankings of posterior probabilities that are robust under changes to such a definition. More specifically, non-parametric Bayesian approaches endow spatial effects with discrete probability distributions using Dirichlet processes, or generalizations thereof, and rely upon computationally intensive methods for inferring on weakly identified parameters. In this manuscript, we introduce a Bayesian linear regression framework to detect spatial health disparities. This enables us to exploit Bayesian conjugate posterior distributions in a more accessible manner and accelerate computation significantly over existing Bayesian non-parametric approaches. Simulation experiments conducted over a county map of the entire United States demonstrate the effectiveness of our method and we apply our method to a data set from the Institute of Health Metrics and Evaluation (IHME) on age-standardized US county-level estimates of mortality rates across tracheal, bronchus, and lung cancer.

1. INTRODUCTION

We propose methods for reporting spatial disparities on maps. Disparities in health outcomes is a rapidly evolving field within public health (see, e.g., [Rao, 2023](#), and references therein) and spatial variation in health outcomes play a crucial role in detecting health disparities. While the role of spatial data analysis in epidemiological investigations has been extensively documented (see, e.g., [Lawson, 2013](#); [Lawson et al., 2016](#); [Waller and Carlin, 2010](#); [Waller and Gotway, 2004](#), and further references therein), inference pertaining to disparities comprises detecting “boundaries” on disease maps that identify significant differences among neighbors. These difference boundaries delineate regions with significantly different disease mortality and incidence rates and assists in improved geographic allocation of health care resources. In geographic analysis, the problem is often treated as one of “wombling” (see [Fitzpatrick et al., 2010a](#); [Jacquez and Greiling, 2003a,b](#); [Li et al., 2011](#); [Lu and Carlin, 2005](#); [Ma and Carlin, 2007](#), for some algorithmic approaches with applications). Probabilistic model-based approaches aiming to resolve this problem include, but are not limited

to, developments in [Corpas-Burgos and Martinez-Beneito \(2020\)](#); [Hanson et al. \(2015\)](#); [Lee and Mitchell \(2012\)](#); [Li et al. \(2012, 2015\)](#); [Lu et al. \(2007\)](#); [Ma et al. \(2010\)](#) and [Gao et al. \(2023\)](#).

In pursuing a probabilistic learning mechanism for adjacency boundaries on a map from data available as aggregates over regions, as is typical of health administration data, we recognize that administrative boundaries between adjacent regions need not represent health outcomes measured there. In somewhat contrarian manner, the more conspicuous disease mapping models assume that neighboring regions are similar to each other. This runs counter to detecting health disparities, where we seek out differences and not similarities. Therefore, modeling spatial disparities needs to balance underlying spatial similarities based upon geographic proximity with the ability to detect differences among neighbors. [Li et al. \(2015\)](#), [Gao et al. \(2023\)](#) and [Aiello and Banerjee \(2023\)](#), for example, propose classes of models that endow the spatial random effects with a discrete probability law using Dirichlet processes. This allows for nonzero probabilities on spatial random effects being equal to each, which are computed as posterior probabilities and used to classify spatial difference boundaries by controlling a Bayesian false discovery rate (on the lines of [Müller et al., 2007](#)).

We aim to obviate some challenges seen in the aforementioned approaches. For one, the computation of the Bayesian nonparametric models devised for difference boundary analysis is cumbersome with the presence of weakly identifiable parameters that impede convergence of iterative estimation algorithms. A second issue is that, while semi-parametric approaches offer some flexibility, the hierarchical Dirichlet process obscures the spatial dependence between the random effects and makes the inference sensitive to values of hyper-parameters. The analysis presented in [Gao et al. \(2023\)](#) also reveal that such models may not deliver optimal sensitivity and specificity with regard to detection of boundaries. Furthermore, ascertaining difference boundaries using such models take into account only the probability of spatial effects being different from each other and not the differences between such effects. How small differences among neighboring effects translate to higher values of the posterior probabilities of the differences remain unaccounted. And the methods do not offer a defense against the argument that small differences in the values of the spatial effects of adjacent regions need not constitute a disparity.

We exploit conjugate distribution theory for hierarchical models to account for the differences between the values of the spatial effects as well as the posterior probabilities of such differences exceeding a certain threshold. In this regard, we extend the approaches in [Lu and Carlin \(2005\)](#) and [Fitzpatrick et al. \(2010b\)](#), who use only posterior means or spatial residuals to detect differences, to full Bayesian inference using posterior distributions to quantify uncertainty. More specifically, we treat spatial disparities as a multiple comparison problem within a Bayesian inferential paradigm by testing for differences in spatial random effects between neighboring regions. Subsequently, we use posterior probabilities of such differences to detect spatial disparities while accounting for false discoveries with the Bayesian FDR ([Müller et al., 2004](#)).

We provide an outline for the rest of the article. Section 2 discusses the problem of detecting differences between fixed effects in a linear model before we extend to spatial random effects.

Section 3 develops the notion of a difference boundary and demonstrates a meaningful connection to traditional hypothesis testing in the simple linear regression model. Section 4 evaluates our methods using simulations over a map of U.S. counties followed by an analysis of tracheal, bronchus and lung cancer mortality data in Section 5. Section 6 concludes with a brief discussion.

2. TESTING FOR SIGNIFICANT CONTRASTS IN BAYESIAN LINEAR REGRESSION

2.1. Conjugate Normal-Gamma Model. Consider the Bayesian linear regression model

$$y = X\beta + \eta, \quad \eta \sim N_n(0, \sigma^2 V_y), \quad (1)$$

where y is an $n \times 1$ vector of observations, X is an $n \times p$ matrix of predictors, β is the unknown $p \times 1$ vector of corresponding regression coefficients, and V_y is a $n \times n$ covariance matrix that is assumed to be completely specified by the analyst. A customary conjugate prior is

$$\pi(\beta, \sigma^2) = N(\beta \mid M_0 m_0, \sigma^2 M_0) \times \text{IG}(\sigma^2 \mid a_0, b_0), \quad (2)$$

where M_0 is a $p \times p$ prior correlation matrix for β that is fixed, m_0 is a fixed $p \times 1$ vector so that $\mathbb{E}[\beta] = M_0 m_0$, a_0 and b_0 are known shape and rate parameters of the inverse-Gamma prior on σ^2 . Familiar Bayesian calculations yield the joint posterior distribution

$$\pi(\beta, \sigma^2 \mid y) = N(\beta \mid M m, \sigma^2 M) \times \text{IG}(\sigma^2 \mid a, b), \quad (3)$$

where $a = a_0 + \frac{n}{2}$, $b = b_0 + \frac{1}{2} \left(y^T V_y^{-1} y + m_0^T M_0 m_0 - m^T M m \right)$, $M = \left(M_0^{-1} + X^T V_y^{-1} X \right)^{-1}$ and $m = m_0 + X^T V_y^{-1} y$. We study the problem of multiple pairwise comparison within the coefficients β when $p > 2$ and thus devote our attention to studying pairwise contrasts of the form $\beta_i - \beta_j$. The fundamental question is: after observing y , how can we make decisions about β_i being different from β_j for a large number of pairs (i, j) ?

We must clarify how we intend to ascertain if β_i is different from β_j . We are unable to simply use $\mathbb{P}(\beta_i = \beta_j \mid y)$ since $\mathbb{P}(\beta_i = \beta_j \mid y) = 0$ for continuous models, such as (3), regardless of the observed data. Hence, it is not possible to directly evaluate the probability of $\beta_i = \beta_j$. One possibility is to use priors with point masses on the regression coefficients, such as slab-spike priors ([Mitchell and Beauchamp, 1988](#)) and several adaptations using mixture models to meaningfully evaluate $\mathbb{P}(\beta_i = 0 \mid y)$. For example, [Scott and Berger \(2006\)](#) investigate multiple comparisons of normal means to 0 by modeling each null hypothesis as independent Bernoulli trials with an unknown common failure probability. However, there is some difficulty in adopting a similar strategy for testing $\beta_i = \beta_j$ in the regression setting because posterior dependence among the elements of β implies that it would be inappropriate to model the contrasts $\beta_i - \beta_j$ being zero as independent Bernoulli random variables. In other words, hypothesis testing of several contrasts on the regression coefficients is a multiple dependent hypothesis testing problem that prevents us from justifying a conditionally independent hierarchical model.

As it stands, the continuous conjugate prior under the standard Bayesian linear regression model is incompatible with difference probabilities that only consider exact equality. Changing the prior or the model sacrifices the analytical simplicity of the conjugate prior in the Bayesian linear regression setting, so we devote our attention to the third approach by considering a new class of difference probabilities. The goal here is to generate easily interpretable and informative statements about the parameters while also prioritizing model simplicity and computational cost.

2.2. Random Effects under an Augmented Linear System. The model in (1) can be criticized as overly simplistic if, for example, both spatial autocorrelation and unstructured random error substantially contribute to the true data generating mechanism. One model that attempts to address this is the BYM (Besag, York and Mollié) model, first introduced in [Besag et al. \(1991\)](#), which includes both a spatially correlated and unstructured error component as part of a Poisson generalized linear model. However, [Simpson et al. \(2017\)](#) and [Riebler et al. \(2016\)](#) explain the error components are not identifiable and scaling issues complicate interpretation of the variance parameters in the BYM model. We follow the parametric form of the BYM model in [Riebler et al. \(2016\)](#) that ensures identifiable error components and imparts better interpretation. We write this BYM2 model as

$$y = X\beta + \gamma + \eta, \quad \gamma = \sigma\sqrt{\rho}\phi, \quad \phi \sim N_n(0, V_\phi), \quad \eta = \sigma\sqrt{1-\rho}v, \quad v \sim N_n(0, I_n) \quad (4)$$

where ϕ is a $n \times 1$ vector of random effects, $\rho \in (0, 1)$ controls the proportion of the total error attributed to the random effects' variance structure, and V_ϕ is a known positive definite matrix. For subsequent analysis, we specify a conditionally autoregressive (CAR) structure, $V_\phi^{-1} = c(D_W - \alpha W)$, where W is the adjacency matrix, D_W is a diagonal matrix with the diagonal elements $D_{W,ii}$ being the number of neighbors of region i , α is the spatial smoothing parameter, and c is a scaling factor. The parameter σ^2 captures the overall error variance if c is set so that the geometric mean of the marginal prior variances is approximately one, and ρ represents the proportion of total variance attributed to the spatial structure ([Riebler et al., 2016](#)).

If $\pi(\gamma, \beta, \sigma^2, \rho) = N(\gamma | 0, \sigma^2\rho V_\phi) \times N(\beta | M_0 m_0, \sigma^2 M_0) \times \text{IG}(\sigma^2 | a_{\sigma^2}, b_{\sigma^2}) \times \pi(\rho)$ is the prior for the parameters in (4), then it is helpful to express the joint posterior distribution in terms of the augmented model ([Banerjee, 2020](#)),

$$\underbrace{\begin{bmatrix} y \\ M_0 m_0 \\ 0_n \end{bmatrix}}_{y_\star} = \underbrace{\begin{bmatrix} X & I_n \\ I_p & 0_{p \times n} \\ 0_{n \times p} & I_n \end{bmatrix}}_{X_\star} \underbrace{\begin{bmatrix} \beta \\ \gamma \end{bmatrix}}_{\gamma_\star} + \underbrace{\begin{bmatrix} \eta \\ \eta_\beta \\ \eta_\phi \end{bmatrix}}_{\eta_\star}, \quad \eta_\star \sim N_{2n+p} \left(0_{2n+p}, \sigma^2 V_{y_\star} \right), \quad (5)$$

where $V_{y_\star} = \begin{bmatrix} (1-\rho)I_n & 0 & 0 \\ 0 & M_0 & 0 \\ 0 & 0 & \rho V_\phi \end{bmatrix}$ and a prior $\pi(\gamma_\star, \sigma^2, \rho) = \text{IG}(\sigma^2 | a_{\sigma^2}, b_{\sigma^2}) \times \pi(\rho)$ (since the prior for $\gamma_\star = (\beta^\top, \gamma^\top)^\top$ has been absorbed into the linear system). The resulting conditional

posterior joint distribution, $\pi(\gamma_\star, \sigma^2 | y, \rho)$, is

$$\pi(\gamma_\star, \sigma^2 | y, \rho) = N_{n+p} \left(\gamma_\star | M_\star m_\star, \sigma^2 M_\star \right) \times \text{IG} \left(\sigma^2 | a_n, b_n \right), \quad (6)$$

where $M_\star = (X_\star^\top V_{y_\star}^{-1} X_\star)^{-1}$, $m_\star = X_\star^\top V_{y_\star}^{-1} y_\star = \left(\frac{1}{1-\rho} y^\top X + m_0^\top, \frac{1}{1-\rho} y^\top \right)^\top$, $a_n = a_{\sigma^2} + \frac{n}{2}$, and $b_n = b_{\sigma^2} + \frac{1}{2} \left(\frac{1}{1-\rho} y^\top y + m_0^\top M_0 m_0 - m_\star^\top M_\star m_\star \right)$. An alternate representation that is interpreted in terms of least squares regression expresses $M_\star m_\star = \widehat{\gamma}_\star$ as the general least square regression estimate solving $X_\star^\top V_{y_\star}^{-1} X_\star \widehat{\gamma}_\star = X_\star^\top V_{y_\star}^{-1} y_\star$ and the scale parameter $b_n = b_{\sigma^2} + \frac{ns^2}{2}$, where $s^2 = \frac{1}{n} (y_\star - X_\star \widehat{\gamma}_\star)^\top V_{y_\star}^{-1} (y_\star - X_\star \widehat{\gamma}_\star)$ is the mean of the residual sums of squares for the linear model in (5).

If $\rho \in (0, 1)$ is fixed, then we can draw exact samples from the joint posterior. Denote $A = X^\top X + (1-\rho)M_0^{-1}$ and $B = \frac{1-\rho}{\rho}V_\phi^{-1} + I_n - XA^{-1}X^\top$. Familiar calculations yield $\text{Var}(\gamma | y, \sigma^2, \rho) = \sigma^2(1-\rho)B^{-1}$, $\text{Var}(\beta | y, \sigma^2, \rho) = \sigma^2(1-\rho)(A^{-1} + A^{-1}X^\top B^{-1}XA^{-1})$, and $\text{Cov}(\beta, \gamma | y, \sigma^2, \rho) = -\sigma^2(1-\rho)A^{-1}X^\top B^{-1}$. Similarly, from $\mathbb{E}[\gamma_\star | y, \sigma^2, \rho] = M_\star m_\star$ we obtain $\mathbb{E}[\beta | y, \sigma^2, \rho] = A^{-1}(X^\top y + (1-\rho)m_0) - A^{-1}X^\top B^{-1}(y - XA^{-1}X^\top y - (1-\rho)XA^{-1}m_0)$ and $\mathbb{E}[\gamma | y, \sigma^2, \rho] = B^{-1}(y - XA^{-1}X^\top y - (1-\rho)XA^{-1}m_0)$. Since $\gamma = \sigma\sqrt{\rho}\phi$, we have

$$\text{Var}(\phi | y, \sigma^2, \rho) = \left(V_\phi^{-1} + \frac{\rho}{1-\rho} (I_n - XA^{-1}X^\top) \right)^{-1}. \quad (7)$$

A flat prior on β considerably simplifies $\mathbb{E}[\gamma^* | y, \sigma^2, \rho]$ and $\text{Var}[\gamma^* | y, \sigma^2, \rho]$. If $\pi(\gamma, \beta, \sigma^2) = N_n(\gamma | 0, \sigma^2 \rho V_\phi) \times \text{IG}(\sigma^2 | a_{\sigma^2}, b_{\sigma^2})$, then $B = \frac{1-\rho}{\rho}V_\phi^{-1} + I_n - H$, where $H = X(X^\top X)^{-1}X^\top$, $\mathbb{E}[\beta | y, \sigma^2, \rho] = (X^\top X)^{-1}X^\top y - (X^\top X)^{-1}X^\top B^{-1}(I - H)y$, $\text{Var}(\beta | y, \sigma^2, \rho) = \sigma^2(1-\rho)(X^\top X)^{-1} + \sigma^2(1-\rho)(X^\top X)^{-1}X^\top B^{-1}X(X^\top X)^{-1}$, $\mathbb{E}[\gamma | y, \sigma^2, \rho] = B^{-1}(I - H)y$, $\text{Var}(\gamma | y, \sigma^2, \rho) = \sigma^2(1-\rho)B^{-1}$, and $\text{Cov}(\beta, \gamma | y, \sigma^2, \rho) = -\sigma^2(1-\rho)(X^\top X)^{-1}X^\top B^{-1}$. Since $\gamma = \sigma\sqrt{\rho}\phi$, we obtain

$$\text{Var}(\phi | y, \sigma^2, \rho) = \left(V_\phi^{-1} + \frac{\rho}{1-\rho} (I_n - X(X^\top X)^{-1}X^\top) \right)^{-1}. \quad (8)$$

In (4), inference on differences within the fixed effects β and the spatial residuals γ are equivalent problems if ρ is known. This implies that a decision framework for the Bayesian fixed effects model specified in (1) can be extended to draw inference on both fixed and random effects in the model given by (4) after conditioning on ρ and V_ϕ . Thus, we turn to the original problem of computing difference probabilities in the fixed effects model before extending to spatial disparities.

2.3. Limiting cases. The limits of the conditional posterior distribution of (β, γ) as $\rho \rightarrow 0^+$ or as $\rho \rightarrow 1^-$ can be analytically derived when the prior is non-informative on β . By the spectral decomposition, $V_\phi^{1/2}(I - H)V_\phi^{1/2} = CDC^\top$ where C is an orthogonal matrix and $D = \text{diag}(d_1, \dots, d_n)$ with entries that are the non-negative eigenvalues of $V_\phi^{1/2}(I - H)V_\phi^{1/2}$. Let $U = V_\phi^{1/2}C$, then U is invertible, $U^\top V_\phi^{-1}U = I_n$, $U^\top(I - H)U = D$, $(1-\rho)B^{-1} = U \left(\frac{1}{\rho}I_n + \frac{1}{1-\rho}D \right)^{-1} U^\top$, and $B^{-1}(I - H) = U \left(\frac{1-\rho}{\rho}I_n + D \right)^{-1} DU^{-1}$. Here, U does not depend on ρ and $\left(\frac{1}{\rho}I_n + \frac{1}{1-\rho}D \right)^{-1}$ is diagonal with

elements $\left(\frac{1}{\rho}I_n + \frac{1}{1-\rho}D\right)_{ii}^{-1} = \left(\frac{1}{\rho} + \frac{d_i}{1-\rho}\right)^{-1}$ and we immediately obtain $\lim_{\rho \rightarrow 0^+} \left(\frac{1}{\rho}I_n + \frac{1}{1-\rho}D\right)^{-1} = 0_{n \times n}$. Next, $B^{-1}(I - H) = U \left(\frac{1-\rho}{\rho}I_n + D\right)^{-1} DU^{-1}$, where $\left(\left(\frac{1-\rho}{\rho}I_n + D\right)^{-1} D\right)_{ii} = d_i \left(\frac{1-\rho}{\rho} + d_i\right)^{-1}$ which is 0 for any $\rho \in (0, 1)$ if $d_i = 0$, and converges to 0 as $\rho \rightarrow 0^+$ if $d_i > 0$. Thus, $\lim_{\rho \rightarrow 0^+} \left(\left(\frac{1-\rho}{\rho}I_n + D\right)^{-1} D\right) = 0_{n \times n}$. These imply that if the prior is non-informative on β , then $\lim_{\rho \rightarrow 0^+} \pi(\beta, \gamma, \sigma^2 | y, \rho)$ collapses to the degenerate mass at $\gamma = 0_n$.

Turning to $\rho \rightarrow 1^-$, we note that if $d_i = 0$, $\left(\frac{1}{\rho}I_n + \frac{1}{1-\rho}D\right)_{ii}^{-1} = \rho$, which converges to 1 as $\rho \rightarrow 1^-$. If $d_i > 0$, then $\lim_{\rho \rightarrow 1^-} \left(\frac{1}{\rho} + \frac{d_i}{1-\rho}\right)^{-1} = 0$ and $\lim_{\rho \rightarrow 1^-} d_i \left(\frac{1-\rho}{\rho} + d_i\right)^{-1} = 1$. Thus, $\lim_{\rho \rightarrow 1^-} \left(\frac{1}{\rho}I_n + \frac{1}{1-\rho}D\right)^{-1} = I_n - D^*$ and $\lim_{\rho \rightarrow 1^-} \left(\frac{1-\rho}{\rho}I_n + D\right)^{-1} D = D^*$ where $D^* \in \mathbb{R}^{n \times n}$ is diagonal with $D_{ii}^* = I(d_i > 0)$ for $i = 1, \dots, n$. Further simplifications reveal that $\lim_{\rho \rightarrow 1^-} \mathbb{E}[\beta | y, \sigma^2, \rho] = (X^T X)^{-1} X^T (y - UD^* U^{-1} e)$, and $\lim_{\rho \rightarrow 1^-} \mathbb{E}[\gamma | y, \sigma^2, \rho] = UD^* U^{-1} e$, where $e = (I - H)y$. Second order moments have limits given by $\lim_{\rho \rightarrow 1^-} \text{Var}(\beta | y, \sigma^2, \rho) = \sigma^2 (X^T X)^{-1} X^T V X (X^T X)^{-1}$, $\lim_{\rho \rightarrow 1^-} \text{Var}(\gamma | y, \sigma^2, \rho) = \sigma^2 V$, and $\lim_{\rho \rightarrow 1^-} \text{Cov}(\beta, \gamma | y, \sigma^2, \rho) = -\sigma^2 (X^T X)^{-1} X^T V$ where $V = V_\phi - UD^* U^T$. Furthermore, $\lim_{\rho \rightarrow 1^-} b_n = b_{\sigma^2} + \frac{1}{2} v^T D^* v$, where $v = U^{-1} e$ (see Section S1). Therefore, $\lim_{\rho \rightarrow 1^-} \pi(\sigma^2 | y, \rho) = \text{IG}(\sigma^2 | a_{\sigma^2} + n/2, b_{\sigma^2} + v^T D^* v/2)$.

3. A NEW FRAMEWORK FOR DETECTING SPATIAL DISPARITIES

3.1. Connection to Classical Hypothesis Testing. Whereas $\mathbb{P}(c_k^T \beta = 0 | y) = 0$ for a continuous posterior distribution, we can test a point null hypotheses $H_0^{(k)} : c_k^T \beta = 0$ against $H_1^{(k)} : c_k^T \beta \neq 0$ for K non-zero $p \times 1$ vectors $c_1, \dots, c_K \in \mathbb{R}^p$ using the classical linear model, $Y = X\beta + \eta, \eta \sim N_n(0_n, \sigma^2 V_y)$, where β is a fixed but unknown $p \times 1$ vector (see, e.g., [Seber and Lee, 2003](#)). For each c_k , this goal is accomplished by computing the test statistic $t_{\text{obs}}^{(k)} = \frac{c_k^T \widehat{\beta}}{\widehat{\sigma} \sqrt{c_k^T (X^T V_y^{-1} X)^{-1} c_k}}$, where $\widehat{\beta} = (X^T V_y^{-1} X)^{-1} X^T V_y^{-1} y$ and $\widehat{\sigma}^2 = \frac{1}{n-p} (y - X\widehat{\beta})^T V_y^{-1} (y - X\widehat{\beta})$ are the generalized least squares estimates. The classical approach computes a p-value $p_k = \mathbb{P}\left(T > \left|t_{\text{obs}}^{(k)}\right|\right)$ where $T \sim t_{n-p}$ and accounts for multiple testing by computing adjusted p-values. If the adjusted p-value is below a pre-specified significance threshold, then $H_0^{(k)}$ is rejected.

In the Bayesian framework, which we adopt here, we maintain the continuous conjugate prior specified by (2) and recast the decision problem to consider the posterior probabilities of absolute standardized linear combinations among elements of β being greater than a threshold ϵ . For all $k = 1, \dots, K$ and any $\epsilon > 0$, we define

$$v_k(\epsilon) = \mathbb{P}\left(\frac{|c_k^T \beta|}{\sigma \sqrt{c_k^T M c_k}} > \epsilon \mid y\right). \quad (9)$$

We refer to these posterior probabilities as ϵ -difference probabilities, where ϵ represents a universal threshold across all K linear combinations and represents the number of posterior standard deviation units that $|c_k^T \beta|$ is away from zero. If $\beta^{(1)}, \dots, \beta^{(N)}$ and $\sigma^{(1)}, \dots, \sigma^{(N)}$ are N samples drawn from their respective posterior distributions, then we estimate (9) using

$$\widehat{v}_k(\epsilon) = \frac{1}{N} \sum_{t=1}^N \mathbf{I} \left(\frac{|c_k^T \beta^{(t)}|}{\sigma^{(t)} \sqrt{c_k^T M c_k}} > \epsilon \right) \quad (10)$$

for any given ϵ . Using a conjugate prior, we efficiently obtain exact posterior samples of $\beta | y$ using (3). Specific domain applications may provide further insights into possible constraints on ϵ and what is considered to be a clinically meaningful difference between coefficients β_i and β_j , which may, for example, represent mean outcomes for different treatment groups in an ANOVA.

Classical p-values and the probabilities $\{v_k(\epsilon)\}_k$ defined in (9) have opposite interpretation: a small p-value, say p_k , suggests $|c_k^T \beta|$ is far from 0, while small $v_k(\epsilon)$ suggests $|c_k^T \beta|$ is likely to be close to 0. The posterior distribution of β with a flat prior is connected to the generalized least squares estimate $\widehat{\beta}$ in the Bayesian linear regression model. Hence, with a specific prior, the p-values and ϵ -difference probabilities are perfectly correlated.

Theorem 1. *Let $c_1, \dots, c_K \in \mathbb{R}^p$, $X \in \mathbb{R}^{n \times p}$, $y \in \mathbb{R}^n$, and $V_y \in \mathbb{R}^{n \times n}$ be fixed. Under the standard linear model $y \sim N_n(X\beta, \sigma^2 V_y)$, let p_k be the p-value for testing the null hypothesis $H_0^{(k)} : c_k^T \beta = 0$ against $H_1^{(k)} : c_k^T \beta \neq 0$ for $k = 1, \dots, K$. Then, $p_k > p_{k'}$ if and only if $v_k(\epsilon) < v_{k'}(\epsilon)$ for all $k \neq k'$, where $v_k(\epsilon) = \mathbb{P} \left(\frac{|c_k^T \beta|}{\sigma \sqrt{c_k^T M c_k}} > \epsilon \mid y \right)$ under $\pi(\beta, \sigma^2) \propto \pi(\sigma^2)$ for any given $\epsilon > 0$.*

Proof. See Appendix A.

For the linear model, the Bayesian approach of ranking ϵ -difference probabilities can replicate the rankings of the classical p-values by using a flat β prior. Theorem 1 implies that the ascending order of the p-values associated with null hypotheses of the form $H_0^{(k)} : c_k^T \beta = 0$ with two-sided alternative $H_1^{(k)} : c_k^T \beta \neq 0$ is equivalent to the descending order of the Bayesian ϵ -difference probabilities. Since this result holds for all $\epsilon > 0$ and the classical procedure does not depend on ϵ , the Bayesian rankings are stable with respect to ϵ .

3.2. Extension to Spatial Random Effects. We next consider the model in (4), where each observation corresponds to one areal region. We treat V_ϕ as a fixed random effects variance structure, whereas ρ , which controls the proportion of the total error variance attributed to the structured component, can either be a fixed hyperparameter or a random variable with a prior density. Generalizing the idea of ϵ -difference probabilities in the fixed effects model, we now conduct posterior inference on random variables of the form $r_k(\epsilon) = \mathbf{I} \left(\frac{|c_k^T \gamma_\star|}{\sigma \sqrt{c_k^T M_\star c_k}} > \epsilon \right)$, for any

given $\epsilon > 0$. For $k = 1 \dots, K$, we define the conditional posterior probability

$$h_k(\epsilon; \rho) = \mathbb{P} \left(\frac{|c_k^\top \gamma_\star|}{\sigma \sqrt{c_k^\top M_\star c_k}} > \epsilon \mid y, \rho \right), \quad (11)$$

where $c_k \in \mathbb{R}^{n+p}$ is typically a contrast on $\gamma_\star = (\beta^\top, \gamma^\top)^\top$. If $c_k^\top \gamma_\star = a_k^\top \gamma$ for some $a_k \in \mathbb{R}^n$, then $h_k(\epsilon; \rho) = \mathbb{P} \left(\frac{|a_k^\top \phi|}{\sqrt{a_k^\top \text{Var}(\phi \mid y, \sigma^2, \rho) a_k}} > \epsilon \mid y, \rho \right)$ where $\text{Var}(\phi \mid y, \sigma^2, \rho)$ is given by (7).

In the context of detecting spatial disparities, consider a set of K pairs of neighboring regions denoted as $L = \{(i, j) : i < j, i \sim j\}$ where $i \sim j$ means that regions i and j are neighbors. If $c_{ij} \in \mathbb{R}^{n+p}$ and $a_{ij} \in \mathbb{R}^n$ such that $c_{ij}^\top \gamma_\star = a_{ij}^\top \gamma = \gamma_i - \gamma_j$, then we denote the corresponding ϵ -difference probability as $h_{ij}(\epsilon; \rho) = \mathbb{P} \left(\frac{|\phi_i - \phi_j|}{\sqrt{a_{ij}^\top \text{Var}(\phi \mid y, \sigma^2, \rho) a_{ij}}} > \epsilon \mid y, \rho \right)$. The set $\{h_{ij}(\epsilon; \rho)\}_{(i,j) \in L}$ then represents the ϵ -difference probabilities of all boundaries under consideration.

According to the equivalence between the model given by (4) and the augmented linear system discussed in Section 2.2, similar insight to the proof of Theorem 1 reveals that the rankings of the conditional posterior probabilities $h_1(\epsilon), \dots, h_K(\epsilon)$ are stable with respect to ϵ for any $\rho \in (0, 1)$.

Theorem 2. *Let $c_1, \dots, c_K \in \mathbb{R}^{n+p}$, $X \in \mathbb{R}^{n \times p}$, and $y \in \mathbb{R}^n$ be known, and consider the model in (4) with prior $\pi(\gamma, \beta, \sigma^2) = N_n(\gamma \mid 0, \sigma^2 \rho V_\phi) \times N_p(\beta \mid M_0 m_0, \sigma^2 M_0) \times IG(\sigma^2 \mid a_{\sigma^2}, b_{\sigma^2})$. Define $h_k(\epsilon; \rho) = \mathbb{P} \left(\frac{|c_k^\top \gamma_\star|}{\sigma \sqrt{c_k^\top M_\star c_k}} > \epsilon \mid y, \rho \right)$ for $k = 1, \dots, K$, any $\epsilon > 0$ and $\rho \in (0, 1)$. For each $k \neq k'$, if there exists $\epsilon_\star > 0$ such that $h_k(\epsilon_\star; \rho) < h_{k'}(\epsilon_\star; \rho)$, then $h_k(\epsilon; \rho) < h_{k'}(\epsilon; \rho)$ for all $\epsilon > 0$.*

Proof. See Appendix B.

If ρ is unknown with a prior distribution $\pi(\rho)$, then the marginal posterior distribution of γ_\star is not analytically accessible. We still define the ϵ -difference probability for the BYM2 model as

$$v_k(\epsilon) = \mathbb{P} \left(\frac{|c_k^\top \gamma_\star|}{\sigma \sqrt{c_k^\top (X_\star^\top V_{y_\star}^{-1} X_\star)^{-1} c_k}} > \epsilon \mid y \right) = \int_0^1 h_k(\epsilon; \rho) \pi(\rho \mid y) d\rho, \quad (12)$$

for any $c_k \in \mathbb{R}^{n+p}$. Given posterior samples $\gamma_\star^{(1)}, \dots, \gamma_\star^{(N)}$ and $\rho^{(1)}, \dots, \rho^{(N)}$, we estimate (12) by

$$\hat{v}_k(\epsilon) = \frac{1}{N} \sum_{t=1}^N \mathbb{I} \left(\frac{|c_k^\top \gamma_\star^{(t)}|}{\sigma^{(t)} \sqrt{c_k^\top \left(X_\star^\top \left(V_{y_\star}^{(t)} \right)^{-1} X_\star \right)^{-1} c_k}} > \epsilon \right), \quad (13)$$

where $V_{y_\star}^{(t)} = \begin{bmatrix} (1 - \rho^{(t)})I_n & 0 & 0 \\ 0 & M_0 & 0 \\ 0 & 0 & \rho^{(t)}V_\phi \end{bmatrix}$. Since $V_{y_\star}^{(t)}$ depends on the sampled value of $\rho^{(t)}$,

computing $\text{Var}(\gamma_\star | y, \sigma^2, \rho)$ for each posterior sample requires inverting an $(n+p) \times (n+p)$ matrix for each posterior sample, which may grow cumbersome. When we are only interested in linear combinations of the spatial effects γ , computation of $\text{Var}(\phi | y, \sigma^2, \rho)$ is sped up significantly by simultaneous reduction and a flat prior on β . By spectral decomposition, $V_\phi^{1/2}(I-H)V_\phi^{1/2} = CDC^\top$, where C is orthogonal and D is diagonal with entries equal to the eigenvalues of $V_\phi^{1/2}(I-H)V_\phi^{1/2}$.

Set $U = V_\phi^{1/2}C$, then by (8), $\text{Var}(\phi | y, \sigma^2, \rho) = U \left(I_n + \frac{\rho}{1-\rho} D \right)^{-1} U^\top$.

The choice of $\pi(\rho)$ is crucial for efficiently sampling from the joint posterior of $\{\beta, \gamma, \sigma^2, \rho\}$ using MCMC and computing (13). Non-informative priors, such as a uniform distributions on $[0, 1]$, induce extreme posterior over-fitting in overly parameterized models (Gelman, 2006; Simpson et al., 2017). Instead, we consider the class of penalized complexity (PC) priors introduced in Simpson et al. (2017) as a means to encourage model parsimony and construct priors imparting better interpretation. We follow Riebler et al. (2016) by placing a PC prior on ρ , denoted by $PC(\rho; \lambda, V_\phi) \propto \lambda \exp(-\lambda d(\rho; V_\phi))$ for $0 \leq \rho \leq 1$, where $\lambda > 0$ is a fixed hyperparameter, $d(\rho; V_\phi) = \sqrt{2D_{KL}(p(y; \rho) || q(y))}$ and $D_{KL}(p(y; \rho) || q(y))$ is the Kullback-Leiber Divergence between $p(y; \rho) = N_n(y | 0_n, \rho V_\phi + (1 - \rho)I_n)$ to the base model with no structured variance $q(y) = N_n(y_{OLS} | 0_n, I_n)$. The hyperparameter λ is chosen such that $P(\rho \leq U) = a$ where U and a are constants. Riebler et al. (2016) presents promising simulation results demonstrating the PC prior's ability to shrink towards the simpler models with only spatial or non-spatial error variance.

When $\pi(\beta, \gamma, \sigma^2, \rho) = N_n(\gamma | 0, \sigma^2 \rho V_\phi) \times \text{IG}(\sigma^2 | a_{\sigma^2}, b_{\sigma^2}) \times PC(\rho | \lambda_\rho, V_\phi)$, Algorithm 1 provides Gibbs update steps for $\{\beta, \gamma, \sigma^2\}$ and a Metropolis-Hastings update step for ρ . Here, `chol` returns the upper triangular Cholesky factor of a positive definite input matrix, `updateBeta` returns β from the full conditional $\beta | y, \gamma, \sigma^2, \rho \sim N_p \left((X^\top X)^{-1} X^\top (y - \gamma), \sigma^2 (1 - \rho) (X^\top X)^{-1} \right)$, `updateGamma` samples $\gamma | y, \beta, \sigma^2, \rho \sim N_n \left(\mu_\gamma, \sigma^2 \left(\frac{1}{1-\rho} I_n + \frac{1}{\rho} V_\phi^{-1} \right)^{-1} \right)$, where $B = \frac{1-\rho}{\rho} V_\phi^{-1} + I - H$ and $\mu_\gamma = B^{-1} \left(y - X (X^\top X + X^\top B^{-1} X)^{-1} (X^\top X \beta + X^\top B^{-1} y) \right)$, and `updateSigmaSq` samples $\sigma^2 | y, \beta, \gamma, \rho \sim \text{InvGamma} \left(a_{\sigma^2} + \frac{n}{2}, b_{\sigma^2} + \frac{\|y - X\beta - \gamma\|^2}{2(1-\rho)} \right)$. `MHupdateRho` updates ρ using a Metropolis-Hastings random walk by proposing $1 - \rho_\star \sim \text{TruncInvGamma} \left(\frac{n}{2}, \frac{\|y - X\beta - \gamma\|^2}{2\sigma^2}, [0, 1] \right)$, which simplifies the acceptance probability calculation. We denote a random variable $X \sim \text{TruncInvGamma}(\alpha, \beta, [c_1, c_2])$, $\alpha > 0, \beta > 0, 0 \leq c_1 < c_2$ if $\mathbb{P}(X \leq x) = \mathbb{P}(Y \leq x | c_1 \leq Y \leq c_2)$, where $Y \sim \text{IG}(\alpha, \beta)$. Computational efficiency is obtained through simultaneous reduction in Algorithm 2 before using the update steps in Algorithm 1 to draw posterior samples of $\{\beta, \gamma, \sigma^2, \rho\}$ in a Metropolis within Gibbs sampling scheme. Samples of ϕ are obtained by using the relation $\phi = \frac{\gamma}{\sigma\sqrt{\rho}}$ with posterior samples of γ, σ^2 , and ρ .

Algorithm 1: Update steps for Metropolis within Gibbs sampling of posterior of $(\beta, \gamma, \sigma^2, \rho)$ in BYM2 Model with flat β prior and PC ρ prior

Given $y, X, M_1 = X^T X, R = \text{chol}(X^T X), V_\phi^{-1}, M_2 = U^T X, m_1 = X^T y, m_2 = U^T y, P,$

$\Lambda = \text{diag}(\lambda_1, \dots, \lambda_n), D = \text{diag}(d_1, \dots, d_n), a_{\sigma^2}, b_{\sigma^2}, \lambda_\rho:$

function updateBeta(γ, σ^2, ρ):

for $i = 1, \dots, p$ **do**

 | Sample $z_i \sim N(0, \sigma^2(1 - \rho)).$

end

 Set $v_p \leftarrow \text{forwardsolve}(R^T, m_1 - X^T \gamma); \beta \leftarrow \text{backsolve}(R, v_p + z).$

return $\beta.$

function updateGamma(β, σ^2, ρ):

 Set $v_p \leftarrow M_1 \beta + M_2^T \text{diag}\left(\frac{\rho}{1 + \rho(d_i - 1)}\right) m_2.$

 Set $W \leftarrow \text{chol}\left(M_1 + M_2^T \text{diag}\left(\frac{\rho}{1 + \rho(d_i - 1)}\right) M_2\right).$

 Set $v_p \leftarrow \text{forwardsolve}(W^T, v_p); v_p \leftarrow \text{backsolve}(W, v_p).$

for $i = 1, \dots, n$ **do**

 | Sample $z_i \sim N(0, \sigma^2).$

end

 Set $\gamma \leftarrow U \text{diag}\left(\frac{\rho}{1 + \rho(d_i - 1)}\right) (m_2 - M_2 v_p) + P \text{diag}\left(\sqrt{\frac{\rho(1 - \rho)}{\rho + \lambda_i(1 - \rho)}}\right) z.$

return $\gamma.$

function updateSigmaSq(ρ, r^2):

 Sample $\tau^2 \sim \Gamma\left(a_{\sigma^2} + \frac{n}{2}, b_{\sigma^2} + \frac{r^2}{2(1 - \rho)}\right); \text{ set } \sigma^2 \leftarrow 1/\tau^2.$

return $\sigma^2.$

function MHupdateRho($\gamma, \sigma^2, \rho, r^2$):

 Initialize $\rho_\star \leftarrow 1.$

while $\rho_\star \geq 1$ **do**

 | Sample $\tau^2 \sim \Gamma\left(\frac{n}{2}, \frac{r^2}{2\sigma^2}\right); \text{ set } \rho_\star \leftarrow 1 - 1/\tau^2.$

end

 Set $c_1 \leftarrow \sqrt{\sum_{i=1}^n \left(\frac{\rho}{\lambda_i} - \log\left(\frac{\rho}{\lambda_i} + (1 - \rho)\right)\right)} - n\rho.$

 Set $c_2 \leftarrow \sqrt{\sum_{i=1}^n \left(\frac{\rho_\star}{\lambda_i} - \log\left(\frac{\rho_\star}{\lambda_i} + (1 - \rho_\star)\right)\right)} - n\rho_\star.$

 Set $\alpha_{MH} \leftarrow \frac{n}{2} \log\left(\frac{\rho}{\rho_\star}\right) + \lambda_\rho (c_1 - c_2) + \frac{\gamma^T V_\phi^{-1} \gamma}{2\sigma^2} \left(\frac{1}{\rho} - \frac{1}{\rho_\star}\right).$

 Sample $u \sim \text{Unif}(0, 1).$

if $\log(u) \leq \alpha_{MH}$ **then return** $\rho_\star.$

else return $\rho.$

Algorithm 2: Metropolis within Gibbs sampling of posterior of $(\beta, \gamma, \sigma^2, \rho)$ in BYM2

Model with flat β prior and PC ρ prior

Given $y, X, M_1 = X^T X, R = \text{chol}(X^T X), I - H, V_\phi^{-1}, a_{\sigma^2}, b_{\sigma^2}, \lambda_\rho, \beta^{(0)}, \gamma^{(0)}, \sigma^{2(0)}, \rho^{(0)}$:

Set $U, D, P, \Lambda \leftarrow \text{simulReduce}(V_\phi^{-1}, I - H)$.

Precompute $M_2 = U^T X, m_1 = X^T y, m_2 = U^T y$.

for $t = 1, \dots, T$ **do**

 Set $\beta^{(t)} \leftarrow \text{updateBeta}(\gamma^{(t-1)}, \sigma^{2(t-1)}, \rho^{(t-1)})$.

 Set $\gamma^{(t)} \leftarrow \text{updateGamma}(\beta^{(t)}, \sigma^{2(t-1)}, \rho^{(t-1)})$.

 Set $r^{2(t)} \leftarrow \|y - X\beta^{(t)} - \gamma^{(t)}\|^2$.

 Set $\sigma^{2(t)} \leftarrow \text{updateSigmaSq}(\rho^{(t-1)}, r^{2(t)})$.

 Set $\rho^{(t)} \leftarrow \text{MHupdateRho}(\gamma^{(t)}, \sigma^{2(t)}, \rho^{(t-1)}, r^{2(t)})$.

end

function $\text{simulReduce}(A, B)$:

 Solve spectral decomposition $A = P\Lambda P^T$ and set $A^{-1/2} \leftarrow P\Lambda^{-1/2}P^T$.

 Solve spectral decomposition $A^{-1/2}BA^{-1/2} = CDC^T$ and set $U \leftarrow A^{-1/2}C$.

return U, D, P, Λ .

3.3. A Bayesian FDR-Based Decision Rule. After computing the difference probability $v_k(\epsilon)$ for each linear combination of interest, we wish to account for multiple comparisons before constructing binary decisions because we are not operating under an automatically penalizing mixture model as in [Scott and Berger \(2006\)](#). We specifically consider safeguarding against Type I errors by controlling the false discovery rate (FDR introduced in [Benjamini and Hochberg, 1995](#)), while retaining

power by minimizing the false negative rate (FNR). Thus, we define $\text{FDR} = \frac{\sum_{k=1}^K \mathbb{I}\left(\frac{|c_k^T \gamma_\star|}{\sigma \sqrt{c_k^T M_\star c_k}} \leq \epsilon\right) d_k}{c + \sum_{k=1}^K d_k}$,

$\text{FNR} = \frac{\sum_{k=1}^K \mathbb{I}\left(\frac{|c_k^T \gamma_\star|}{\sigma \sqrt{c_k^T M_\star c_k}} > \epsilon\right) (1 - d_k)}{c + \sum_{k=1}^K (1 - d_k)}$ where $c > 0$ is a small constant to avoid a zero denominator and

$d_k \in \{0, 1\}$ represents our decision to declare $\frac{|c_k^T \gamma_\star|}{\sigma \sqrt{c_k^T M_\star c_k}} > \epsilon$. As explained in [Müller et al. \(2007\)](#), the FDR and FNR functions are random variables that align with neither the classical nor Bayesian paradigm and, hence, have distinct interpretations in the two paradigms.

Given a set of difference probabilities $\{v_1(\epsilon), \dots, v_K(\epsilon)\}$, we use the Bayesian FDR and FNR defined in [Müller et al. \(2004\)](#) as the posterior expectation

$$\overline{\text{FDR}}(t^*, \epsilon) = \mathbb{E}[\text{FDR}(t^*, \epsilon) | y] = \frac{\sum_{k=1}^K (1 - v_k(\epsilon)) \mathbb{I}(v_k(\epsilon) \geq t^*)}{\sum_{k=1}^K \mathbb{I}(v_k(\epsilon) \geq t^*)}, \quad (14)$$

$$\overline{\text{FNR}}(t^*, \epsilon) = \mathbb{E}[\text{FNR}(t^*, \epsilon) | y] = \frac{\sum_{k=1}^K v_k(\epsilon) \mathbb{I}(v_k(\epsilon) < t^*)}{\sum_{k=1}^K \mathbb{I}(v_k(\epsilon) < t^*)}. \quad (15)$$

Minimizing the $\overline{\text{FNR}}$ subject to $\overline{\text{FDR}} \leq \delta$ is achieved by decisions of the form $d_k = \mathbb{I}(v_k(\epsilon) \geq t^*(\epsilon))$, where $t^*(\epsilon) \in [0, 1]$ for all $\epsilon > 0$ is a threshold chosen as

$$t^*(\epsilon) = \inf \left\{ t \in [0, 1] : \overline{\text{FDR}}(t, \epsilon) \leq \delta \right\}. \quad (16)$$

The Bayesian and classical FDR control procedures compute posterior probabilities and p-values, respectively, which are used to rank the plausibility of each hypothesis before choosing a cutoff according to a decision rule. In general, the Bayesian FDR and its classical analogue are fundamentally different criterion that are not necessarily equivalent and their respective control procedures may produce different sets of decisions. However, in the linear fixed effects model and the setting of Theorem 1, if the prior is non-informative on β in the Bayesian approach, then the order of the posterior probabilities is the reversed order of the p-values. In this case, the Bayesian and classical FDR control procedures differ only in the decision criterion; specific choice of the decision parameter δ in the Bayesian approach can afford decisions identical to many classical FDR control procedures.

For creating binary decisions, ϵ must be chosen to apply this Bayesian FDR control procedure. However, for any $\delta > 0$, if we set ϵ to be arbitrarily small and $t^* = 0$, we would declare every decision positive as $d_k = 1$. On the other hand, if we set ϵ to be arbitrarily large and $t^* = 1$, then we would declare every decision negative as $d_k = 0$. Both cases achieve $\overline{\text{FDR}} \leq \delta$ but do not induce meaningful statements about the data. This motivates a heuristic to choose ϵ at a reasonable value before applying the Bayesian FDR control procedure to create decisions.

3.4. Selecting an ϵ -difference threshold. In the absence of guidance on the choice of ϵ , we consider two general heuristics to select a reasonable value for ϵ , the first based on a loss function and the relation between ϵ and our resulting actions. As ϵ increases, the event $\frac{|c_k^T \gamma_\star|}{\sigma \sqrt{c_k^T M_\star c_k}} > \epsilon$ gains stronger meaning, but has a lower posterior probability. On the other hand, the event $\frac{|c_k^T \gamma_\star|}{\sigma \sqrt{c_k^T M_\star c_k}} \leq \epsilon$ becomes less precise but more probable. This motivates the use of a loss function that is optimized with respect to ϵ by balancing the strength of our affirmative conclusions that $\frac{|c_k^T \gamma_\star|}{\sigma \sqrt{c_k^T M_\star c_k}} > \epsilon$ with the precision of our negative conclusions that state $\frac{|c_k^T \gamma_\star|}{\sigma \sqrt{c_k^T M_\star c_k}} \leq \epsilon$.

As a general heuristic, we appeal to the principle of maximum entropy, which suggests that, given a selection of possible posterior distributions, the posterior distribution that best represents our posterior knowledge is precisely the one with maximum entropy. The principle of maximum entropy (Jaynes, 1957) selects the maximum entropy distribution due to it being “maximally noncommittal” with respect to the amount of information we imbue the posterior with beyond the observed data. Under the model (4), choosing an extremely small or large difference threshold ϵ causes the posterior distribution of $r_k(\epsilon) = \mathbb{I}\left(\frac{|c_k^T \gamma_\star|}{\sigma \sqrt{c_k^T M_\star c_k}} > \epsilon\right)$ to collapse into a point mass at 1 or 0 respectively, which has minimal entropy. Maximizing the joint posterior entropy of

$R = \{r_1(\epsilon), \dots, r_K(\epsilon)\}$ with respect to ϵ thus avoids obscuring the information that the data y provides on the true quantities of interest, $\left\{ \frac{|c_1^T \gamma_\star|}{\sigma \sqrt{c_1^T M_\star c_1}}, \dots, \frac{|c_K^T \gamma_\star|}{\sigma \sqrt{c_K^T M_\star c_K}} \right\}$.

Shannon (1948) explains the Shannon entropy as an objective measure of the information or uncertainty of a probability distribution. Let I be a $K \times 1$ vector such that $I_k \in \{0, 1\}$ for all $k = 1, \dots, K$ and let $g(I) = \mathbb{P}(\cap_{k=1}^K r_k(\epsilon) = I_k | y)$. Since $r_k(\epsilon)$ is a binary random variable equal to 1 with posterior probability $v_k(\epsilon)$, the joint Shannon posterior entropy of R measured in nats is defined as $H(R) = -\sum_{I \in \{0,1\}^K} g(I) \log g(I)$. However, the joint entropy entails estimating 2^K probabilities and is computationally unfeasible even for moderate K .

Instead, we opt for maximizing the entropy of a uniformly chosen ϵ -difference indicator. For any $\epsilon > 0$, let J be a random variable with uniform probability mass on $\{1, \dots, K\}$ and $W = r_J(\epsilon)$. The conditional posterior entropy of W given J is $H_J(W) = \sum_{k=1}^K H(r_k(\epsilon)) P(J = k) = \frac{1}{K} \sum_{k=1}^K H(r_k(\epsilon))$. The sum of the individual entropies is related to the joint entropy by the subadditivity property of the joint entropy (Shannon, 1948), which states that $H(R) \leq \sum_{k=1}^K H(r_k(\epsilon)) = -\sum_{k=1}^K v_k(\epsilon) \log v_k(\epsilon) + (1 - v_k(\epsilon)) \log(1 - v_k(\epsilon))$. We obtain an optimal ϵ by maximizing the average of the individual entropies with respect to ϵ or equivalently minimizing the loss function

$$\text{LOSS}_{\text{CE}}(\epsilon) = \sum_{k=1}^K v_k(\epsilon) \log v_k(\epsilon) + (1 - v_k(\epsilon)) \log(1 - v_k(\epsilon)), \quad (17)$$

which we refer to as the conditional entropy loss function. We denote the ϵ obtained from minimizing this loss function as ϵ_{CE} . When $v_k(\epsilon)$ is not available in closed form, this loss function is estimated from the posterior samples using (10). For difference boundary analysis on a set L containing K pairs of neighboring regions and a corresponding set of difference probabilities denoted as $\{v_{ij}(\epsilon)\}_{(i,j) \in L}$, the summation in (17) is over all pairs of neighboring regions, $(i, j) \in L$. $v_k(\epsilon)$ is also replaced with $h_k(\epsilon; \rho)$ as defined in (11) when conditioning on a given $0 < \rho < 1$.

As an alternative to maximizing a loss function based upon conditional entropy, we can consider the number of positive decisions, denoted by T . Fixing two quantities out of ϵ , δ and T determines the third, representing a three-way trade-off between protection against Type I errors, quantity, and quality in our positive results: δ indicates our tolerance for false positives; T is the quantity of positive results; and ϵ is our standard for a disparity, which can be thought as the quality of our decisions. If the maximum allowable Bayesian FDR, δ , and the number of decisions, T , are fixed, then a valid choice of ϵ should belong to $A_\epsilon = \left\{ \epsilon > 0 : \overline{\text{FDR}}(t^\star(\epsilon)) \leq \delta, |S(\epsilon)| \geq T \right\}$. This criterion can be more useful in policy settings aiming to identify rankings of the most egregious disparities, for example, the top fifty. Finally, by fixing ϵ and T , δ implicitly equals the Bayesian FDR of the resulting decisions, although this represents no active protection against Type I errors.

We conclude this section with a remark regarding the implications of the limiting cases discussed in Section 2.3. As ρ tends to 0, boundary detection becomes meaningless because the spatial effects converge to 0. As ρ tends to 1, σ^2 and γ also have limiting distributions described at the end of

Section 2.3. These results suggest that the conditional variance of γ (used in the definition of the ϵ -difference probability) or σ^2 will neither blow up nor shrink to nearly 0 when ρ is near 1.

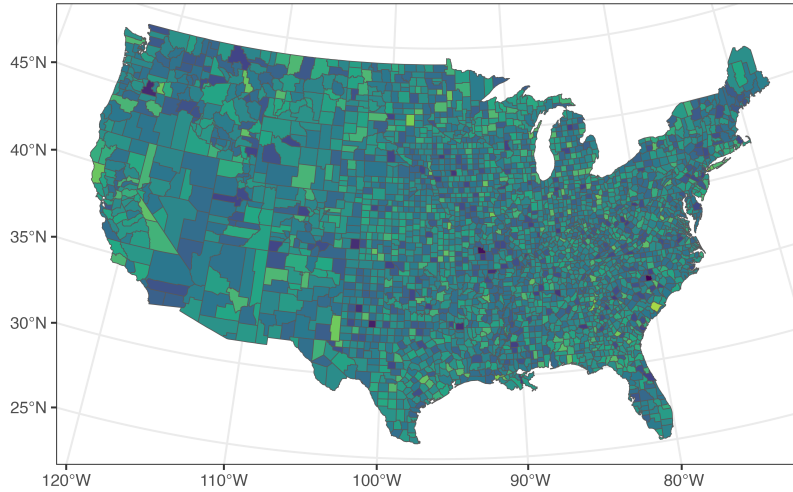
4. SIMULATION EXPERIMENTS

4.1. Exact Conjugate BYM2 Model. To assess the performance of our proposed framework for detecting spatial disparities, we conduct a simulation experiment by generating data over 3,078 contiguous U.S. counties. We first investigate an exact sampling scheme that conditions on a fixed value of ρ and places a conditionally autoregressive (CAR) structure on the precision matrix of the spatial random effects. In the model given by (4), we construct $V_\phi^{-1} = c(D_W - \alpha W)$ using the neighborhood relations of the U.S. counties and generate the spatial random effects ϕ using $\alpha = 0.99$, scaling factor $c = 0.365$, and covariates $X = (1_n, x)$ where $x \sim N_n(0, I_n)$, before simulating the observed data y using (4) with $\sigma^2 = 4$, $\rho = 0.93$, and $\beta = (2, 5)^\top$.

We investigate spatial difference boundary detection on the set of all pairs of neighboring counties, denoted as $L = \{(i, j) : i < j, i \sim j\}$. The indicator of a true spatial disparity for pair (i, j) and a given difference threshold ϵ is defined as $r_{ij}(\epsilon) = \mathbb{I}\left(\frac{|\phi_i - \phi_j|}{\sqrt{c_{ij}^\top \text{Var}(\phi | y, \sigma^2, \rho) c_{ij}}} > \epsilon\right)$, evaluated using the true values of ϕ and ρ . For the simulated data, there are $K = 9,119$ unique neighboring pairs of counties. Using the prior $\pi(\gamma, \beta, \sigma^2) = N(\gamma | 0, \sigma^2 \rho V_\phi) \times N(\beta | M_0 m_0, \sigma^2 M_0) \times \text{IG}(\sigma^2 | a_{\sigma^2}, b_{\sigma^2})$ with $M_0^{-1} = 10^{-4} I_2$, $m_0 = 0_p$, $a_{\sigma^2} = 0.1$, and $b_{\sigma^2} = 0.1$, we generate 10,000 exact samples from the posterior distribution of ϕ extracted from γ in (6). Figure 1 shows the posterior predictive means of the data juxtaposed to the observed values, indicating an excellent fit.

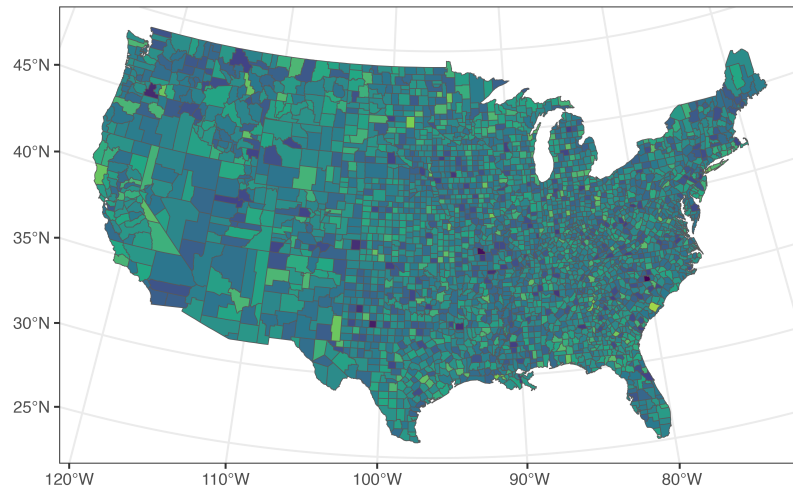
Given $\rho = 0.93$, we use posterior samples of $(\beta, \gamma, \sigma^2)$ to compute Monte Carlo estimates of $\{h_{ij}(\epsilon)\}_{(i,j) \in L}$ as defined in (11), which we treat as the difference probabilities in the conditional entropy loss in (17). By numerically minimizing the conditional entropy loss, we obtain the optimal threshold as $\epsilon_{CE} = 1.296$. Figure 2a displays the loss function evaluated ϵ and Figure 2b displays a histogram of $\{h_{ij}(\epsilon_{CE})\}_{(i,j) \in L}$, showing a cluster of probabilities near 1 that correspond to strong posterior evidence of a spatial disparity with a $\epsilon_{CE} = 1.296$ difference threshold.

After setting the difference threshold at $\epsilon_{CE} = 1.296$, we use the Bayesian FDR control procedure discussed in Section 3.3 to classify boundaries as spatial disparities by considering the conditional posterior probabilities $\{h_{ij}(\epsilon_{CE})\}_{(i,j) \in L}$ as the difference probabilities. We first use the Monte Carlo estimates of $\{h_{ij}(\epsilon_{CE})\}_{(i,j) \in L}$ to estimate the Bayesian FDR and FNR as defined in (14) and (15) respectively before selecting a cutoff posterior probability t_\star according to (16) with Bayesian FDR tolerance $\delta = 0.10$, which results in setting $t_\star = 0.6479$ and declaring 4,540 boundaries as spatial disparities. According to the true values of ϕ , 4,562 out of 9,119 boundaries are a spatial disparity with the same $\epsilon_{CE} = 1.296$ difference threshold. Comparing with true disparities, we achieve approximately 71.2% sensitivity, 86.2% specificity, 76.8% accuracy, a true false discovery rate of 10.2%, and a true false negative rate of 36.3%. As discussed in Section 3.3, the true false



Simulated Y
-20 -10 0 10 20

(A)



Y posterior mean
-20 -10 0 10 20

(B)

FIGURE 1. (a) Simulated response data y where the spatial random effects ϕ are simulated under a scaled CAR variance structure and (b) posterior means of data computed using 10,000 exact samples from the joint posterior.

discovery rate exceeds $\delta = 0.1$ because δ represents tolerance for Bayesian FDR, which is a metric fundamentally different from classical FDR control procedures.

To illustrate the effect of ϵ on the Bayesian FDR and FNR, we evaluate the estimated Bayesian FDR and FNR as functions of the cutoff t for multiple fixed values of ϵ . Figure 3 shows the

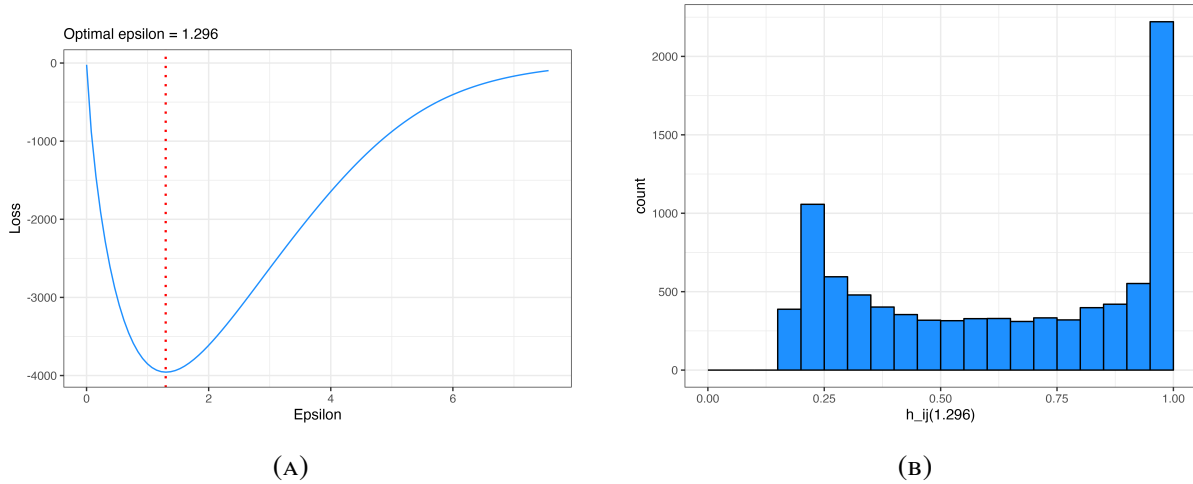


FIGURE 2. (a) Conditional entropy loss function evaluated across ϵ with a dotted line indicating the numerically optimal difference threshold $\epsilon_{CE} = 1.296$. (b) Histogram of the resulting posterior probabilities $\{h_{ij}(\epsilon_{CE})\}_{(i,j) \in L}$.

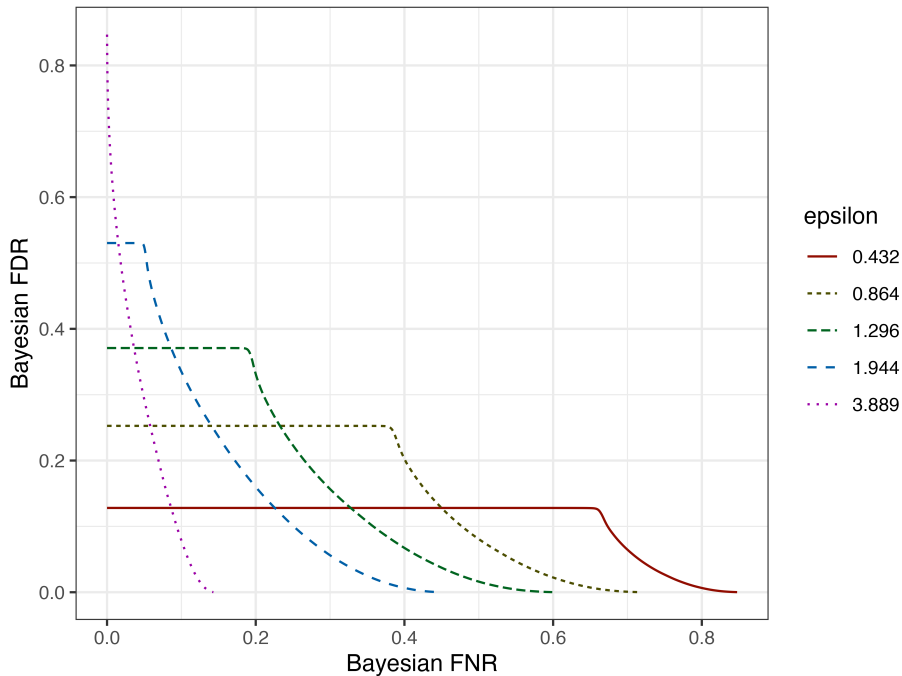


FIGURE 3. Bayesian FDR against FNR curves for different values of ϵ .

FDR versus FNR curves for $\epsilon = 0.432, 0.864, 1.296, 1.944, 3.889$. The goal for any given ϵ is to minimize the Bayesian FNR under the constraint that Bayesian FDR $\leq \delta$, but Figure 3 demonstrates that the FDR versus FNR curve becomes increasingly steep near 0. According to our posterior belief, there are few disparities at a large ϵ level, so both the Bayesian FNR and FDR incentivize

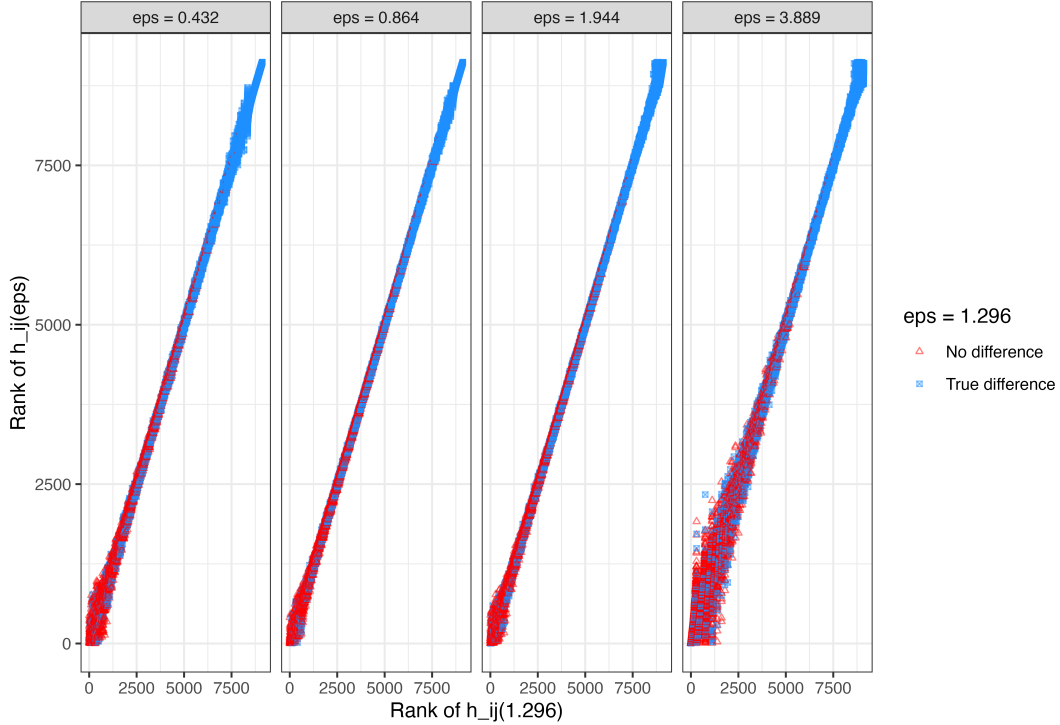


FIGURE 4. Rankings of the simulated difference probabilities $\{h_{ij}(\epsilon)\}_{(i,j)\in L}$ for $\epsilon = 0.432, 0.864, 1.944, 3.889$ versus rankings of $\{h_{ij}(\epsilon_{CE})\}_{(i,j)\in L}$ when conditioning on the true value of ρ . True disparities according to the true values of ϕ and ρ are shown in blue.

declaring few boundaries as disparities. On the other hand, decreasing ϵ causes the FDR versus FNR curve to plateau at a lower FDR value because the event that each difference exceeds the ϵ threshold becomes more probable and occurs with nearly probability one for small enough ϵ . This behavior of the Bayesian FDR and FNR is the motivation of the criteria in Section 3.4 for selecting a reasonable value of ϵ before accounting for multiplicity by controlling the Bayesian FDR.

Since the probabilities $\{h_{ij}(\epsilon_{CE})\}_{(i,j)\in L}$ are computed conditional on exact knowledge of ρ , their rankings are theoretically stable by Theorem 2. Figure 4 displays stable rejection paths of the difference probabilities for values of ϵ surrounding the chosen threshold ϵ_{CE} , but the instability in the low ranks of the rightmost graph are due to imprecise Monte Carlo estimates of posterior probabilities near zero with a large difference threshold, $\epsilon = 3.889$. Figure 4 also shows a separation of the true disparities from the non-disparities at the $\epsilon_{CE} = 1.296$ difference level, demonstrating the efficacy of our method in the exact sampling setting.

4.2. Placing a prior on ρ . In practice, the true value of ρ , the approximate proportion of variance attributable to the spatial CAR structure, is not known. The choice of ρ to condition on can be regarded as a model selection problem, where common approaches are based on information criteria,

such as the DIC as introduced in Spiegelhalter et al. (2002) and the WAIC, introduced by Watanabe (2010). DIC and WAIC values are computed using the predictive distribution $Y | \beta, \gamma, \sigma^2, \rho \sim N_n(X\beta + \gamma, \sigma^2(1 - \rho)I_n)$ and often involve corrections, such as p_{DIC} and p_{WAIC2} , which are discussed in Gelman et al. (2014). However, for the model given by (4) and conditioned on a given $\rho \in (0, 1)$, each metric decreases asymptotically to $-\infty$ as $\rho \rightarrow 1^-$, regardless of the true value of ρ used to generate the data. This is supported both by simulation and analytical arguments in Sections S1 and S2. Gelman et al. (2014) explains that WAIC and DIC estimate the out-of-sample prediction error, which is nearly erased when $\rho \approx 1$ indicates a spatially dominant model with negligible measurement error. Intuitively, the DIC and WAIC metrics cannot account for the overfitting that occurs as $\rho \rightarrow 1^-$ and $\|y - X\beta - \gamma\|^2$ converges in probability to 0.

As we cannot apply model selection techniques based on information criteria using the specified predictive distribution to select a reasonable value of ρ to condition on, we pivot to evaluating posterior inference with a prior on ρ as discussed in Section 3.2 on the same simulation data from Section 4.1. We specify the joint prior as $\pi(\beta, \gamma, \sigma^2, \rho) = N_n(\gamma | 0, \sigma^2 \rho V_\phi) \times \text{IG}(\sigma^2 | a_{\sigma^2}, b_{\sigma^2}) \times \text{PC}(\rho | \lambda_\rho)$, where $a_{\sigma^2} = 0.1$ and $b_{\sigma^2} = 0.1$. For the PC prior on ρ , we follow Riebler et al. (2016) and choose $\lambda_\rho = 0.0335$ such that $\mathbb{P}(\rho < 0.5) \approx \frac{2}{3}$. We then apply Algorithm 2 to draw 30,000 posterior samples of $(\beta, \gamma, \sigma^2, \rho)$ after 10,000 burn-in samples. A 95% credible interval for ρ is (0.867, 0.991), showing that our algorithm can effectively learn about ρ .

Since we are only considering spatial effect differences associated with physical boundaries, the ϵ -difference probability in (12) simplifies to $v_{ij}(\epsilon) = \mathbb{P}\left(\frac{|\phi_i - \phi_j|}{\sqrt{a_{ij}^T \text{Var}(\phi | y, \sigma^2, \rho) a_{ij}}} > \epsilon \mid y\right)$, where $(i, j) \in L$ is a pair of neighboring counties and a_{ij} is a $n \times 1$ vector with 1 in the i th coordinate, -1 in the j th coordinate, and 0 elsewhere. We compute Monte Carlo estimates of $\{v_{ij}(\epsilon)\}_{(i,j) \in L}$ using (13) and minimize the conditional entropy loss function in (17) to obtain $\epsilon_{CE} = 1.611$ as the optimal difference threshold. To compare the classification performance of placing a PC prior on ρ versus fixing ρ as in Section 4.1, we compute the ROC curves for both settings which displays the sensitivity versus specificity. Moving on the ROC curve from left to right can be considered as implicitly decreasing the classification threshold or increasing the Bayesian FDR tolerance δ . Figure 5a shows nearly identical ROC curves for sampling with a fixed ρ and a PC prior on ρ , which indicates similar performance up to the classification threshold. Figure 5b displays the estimated Bayesian FDR versus the true sensitivity for both models, illustrating that placing a prior on ρ also does not significantly impact the behavior of the Bayesian FDR. Figure 5b also suggests that in this simulation, setting $\delta = 0.1$ achieves approximately 70% sensitivity and setting $\delta = 0.05$ achieves approximately 50% sensitivity when placing a PC prior on ρ .

We also evaluate the stability of the rankings of the ϵ -difference probabilities $\{v_{ij}(\epsilon)\}_{(i,j) \in L}$. Figure 6 shows the rejection paths for $\epsilon = 0.537, 1.074, 2.417, 4.833$ against that of $\epsilon_{CE} = 1.611$. The rightmost graph shows that the rankings are slightly shifted when the difference threshold is tripled to $\epsilon = 4.833$, but the rankings remain stable when increasing or decreasing the difference

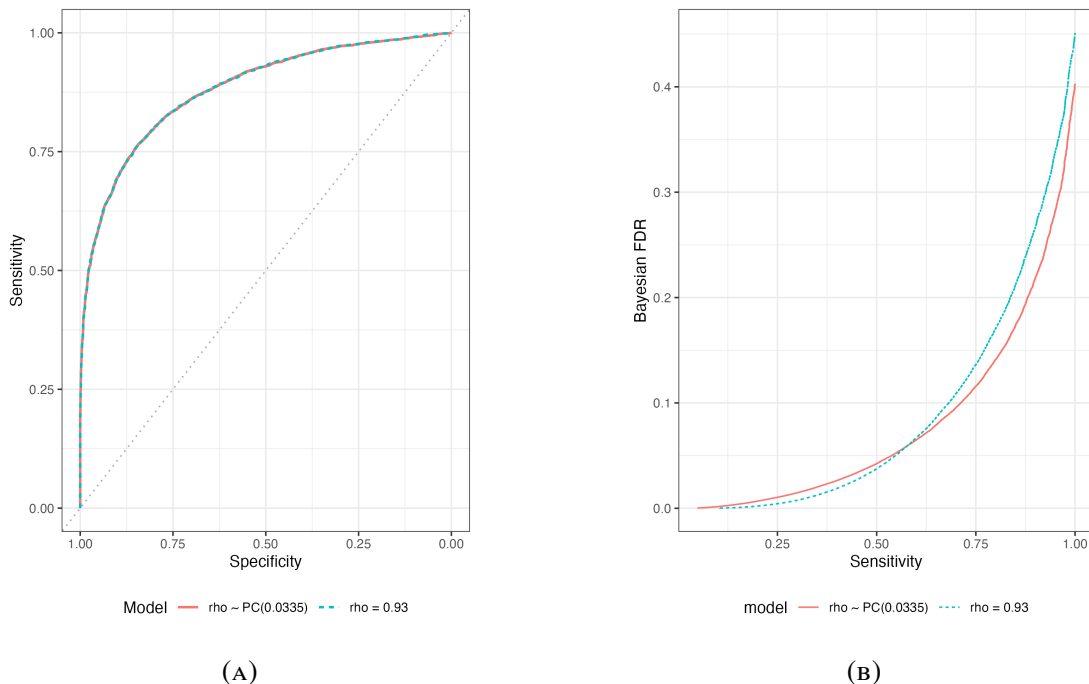


FIGURE 5. Classification performance of spatial disparity detection on simulated data when drawing exact samples conditional on $\rho = 0.93$ versus placing a PC prior on ρ and using Metropolis within Gibbs sampling. The classification performance of both models are compared using fixed difference threshold $\epsilon_{CE} = 1.611$. (a) ROC curves for each model. The area under each ROC curve is 0.881. (b) Bayesian FDR versus true sensitivity.

threshold ϵ_{CE} by 50%. Thus, the rejection path that our method produces in this instance is reasonably robust to selection of the difference threshold ϵ .

5. APPLICATION

As a data analysis example from public health, we apply our method to publicly available data from the Institute of Health Metrics and Evaluation (IHME) on age-standardized US county-level estimates of mortality rates across tracheal, bronchus, and lung cancer in 2014 (Mokdad et al., 2017). We incorporate one predictor, county-level estimates of total (non-daily and daily) smoking prevalence in both sexes in 2012 originally derived using data from the Behavioral Risk Factor Surveillance System in Dwyer-Lindgren et al. (2014). Previous work by (Shreves et al., 2023) indicates that lung cancer mortality rates exhibit spatial autocorrelation that is not completely accounted for by smoking prevalence.

For our study region, we subset to $n = 3,017$ contiguous U.S. counties with available estimates for smoking prevalence and lung cancer mortality rates with the intent of detecting disparities corresponding to county boundaries. Although we drop counties with missing data for the sake

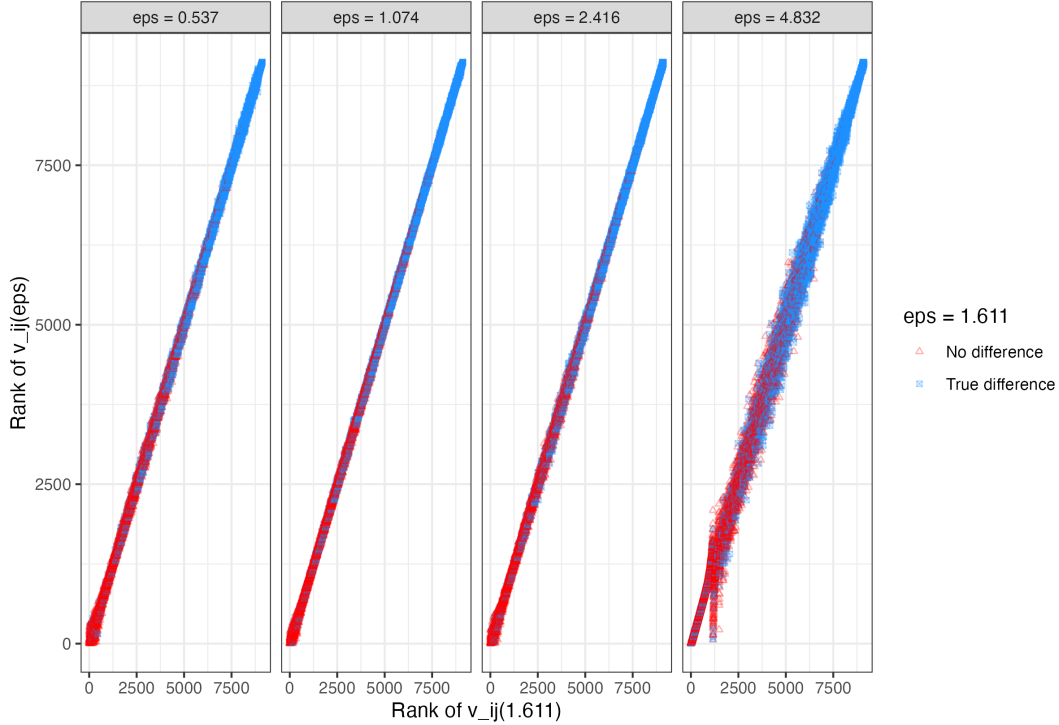
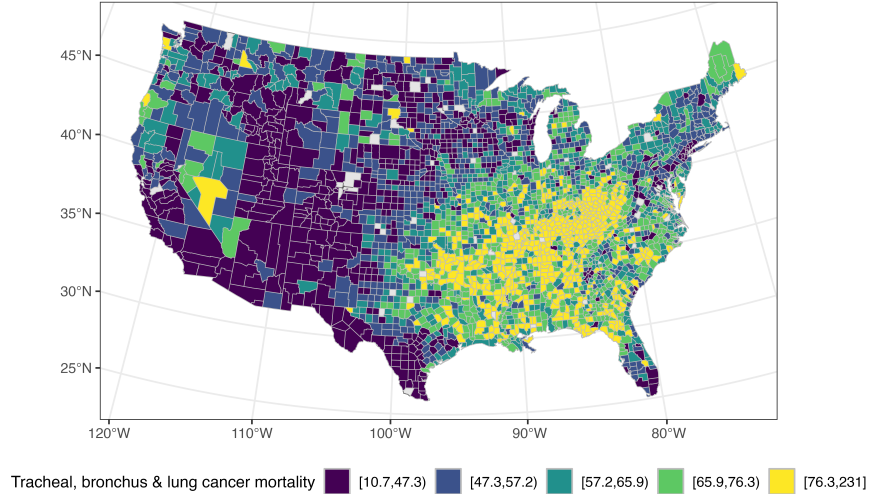


FIGURE 6. Simulated rankings of ϵ -difference probabilities $\{v_{ij}(\epsilon)\}_{(i,j) \in L}$ for $\epsilon = 0.537, 1.074, 2.417, 4.833$ versus rankings of $\{v_{ij}(\epsilon_{CE})\}_{(i,j) \in L}$ using a PC prior on ρ . True disparities according to the true values of ϕ and ρ are shown in blue.

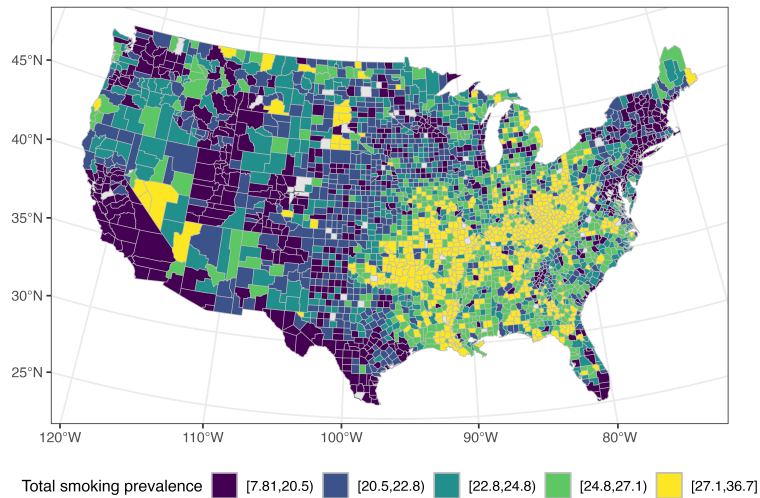
of simplicity here, one can refer to [Rubin \(1976\)](#) for an introduction to Bayesian approaches to missing data or [Ma and Chen \(2018\)](#) for a modern overview. For simplicity, we drop these counties from our study region as the remaining counties form a contiguous region. The cancer mortality rate and total smoking prevalence estimates of the final study region are mapped in Figure 7. High risk regions can clearly be identified most notably in the East South Central states, and our analysis aims to identify local health inequity on the county-level.

To assess spatial autocorrelation in the model, we fit an ordinary least squares linear model with an intercept and smoking prevalence as a predictor of lung cancer mortality before computing Moran's $I = 0.4563$ and Geary's $C = 0.5330$ using the residuals ([Banerjee et al., 2015](#)). Both statistics were highly significant under 10,000 random permutations (p-value = 1/10,001), suggesting that spatial autocorrelation is not fully captured by the linear relationship between smoking prevalence and mortality rates. Therefore, we proceed with analyzing the data under a spatial model.

We consider the data under the model of (4) such that $y | \beta, \gamma, \sigma^2, \rho \sim N_n(X\beta + \gamma, \sigma^2(1 - \rho)I_n)$ where $\beta = (\beta_0, \beta_1)^T$ and β_1 is the linear coefficient of smoking prevalence. Similar to the simulation examples, we place a CAR prior on ϕ by setting $V_\phi^{-1} = c(D_W - \alpha W)$, where the neighbor and adjacency matrices are computed using the subset of U.S. counties, $\alpha = 0.99$, and $c = 0.3762$. We treat ρ as an unknown parameter and specify the joint prior as $\pi(\beta, \gamma, \sigma^2, \rho) =$



(A)



(B)

FIGURE 7. (a) Map of county-level age-standardized mortality rate estimates across tracheal, bronchus, and lung cancer in 2014, colored by quintile. (b) Map of county-level total smoking prevalence estimates in 2012, colored by quintile.

$N_n(\gamma | 0, \sigma^2 \rho V_\phi) \times \text{IG}(\sigma^2 | a_{\sigma^2}, b_{\sigma^2}) \times \text{PC}(\rho | \lambda_\rho)$, where $a_{\sigma^2} = 0.1$ and $b_{\sigma^2} = 0.1$. Although the set of regions here differs slightly from the simulation example, we also set $\lambda_\rho = 0.0335$ since it approximately satisfies $\mathbb{P}(\rho \leq 0.5) = \frac{2}{3}$.

After 10,000 burn-in samples, we draw 30,000 samples from of the posterior of $\{\beta, \gamma, \sigma^2, \rho\}$ using Algorithm 2. Table 1 presents 95% credible intervals for the non-spatial effect parameters. The credible interval of ρ suggests that we are able to learn effectively about ρ and the CAR spatial model explains a majority of the variance in the data.

Parameter	Description	Mean	95% Credible Interval
β_0	Intercept	9.57	(6.073, 13.205)
β_1	Smoking prevalence	2.24	(2.117, 2.357)
σ^2	Total variance	114.47	(101.506, 131.105)
ρ	Spatial proportion of variance	0.78	(0.704, 0.86)

TABLE 1. Posterior summaries of non-spatial effect parameters.

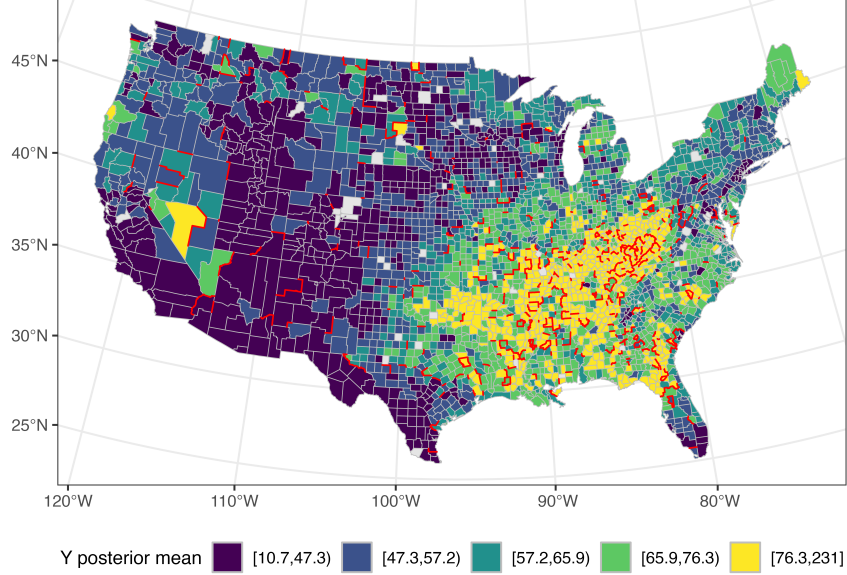


FIGURE 8. Map of posterior means of modeled tracheal, bronchus, and lung cancer mortality rates. Red lines correspond to classified disparities between neighboring counties at difference threshold $\epsilon_{CE} = 0.928$ with Bayesian FDR tolerance $\delta = 0.05$.

We proceed with detecting spatial disparities using the ϵ -difference framework introduced in Section 3. For this dataset, we consider the set of all $K = 8,793$ pairs of neighboring counties, denoted as $L = \{(i, j) : i < j, i \sim j\}$, and ϵ -difference probabilities of the form $v_{ij}(\epsilon) = \mathbb{P}\left(\frac{|\phi_i - \phi_j|}{\sqrt{a_{ij}^T \text{Var}(\phi | y, \sigma^2, \rho) a_{ij}}} > \epsilon \mid y\right)$ for all $(i, j) \in L$. We select the difference threshold ϵ by minimizing the conditional entropy loss in (17), which yields $\epsilon_{CE} = 0.928$. For this analysis example, we set a maximum allowable Bayesian FDR of $\delta = 0.05$, compute $t_\star = 0.882$ using (16), and report 731 county boundaries as a spatial disparity.

To assess the predictive fit, we draw one value of $y_{rep}^{(s)} \sim N_n\left(X\beta^{(s)} + \gamma^{(s)}, \sigma^{2(s)}(1 - \rho^{(s)})I_n\right)$ for each value of the posterior samples $\{\beta^{(s)}, \gamma^{(s)}, \sigma^{2(s)}, \rho^{(s)}\}$. The posterior predictive means along with the classified neighbor disparities are mapped in the lower map of Figure 8. The majority of reported disparities lie in relatively high risk states (KY, GA, TN, WV, MS, MS, MO, VA)

where many county mortality rate estimates lie in the upper quintile with a large range, suggesting that health inequity is prevalent on the local county scale in these regions. This aligns with our intuition that detected disparities would be more abundant in higher-risk regions where geographic variation is more pronounced. The full list of the 731 detected difference boundaries ranked by their corresponding posterior probability is available in Table S1.

6. DISCUSSION

Compared to previous methodology for detecting spatial disparities, our proposed analysis procedure holds a few advantages. Notably, there is a clear difference in interpretation between our definition of the boundary probability compared to Bayesian non-parametric approaches that utilize Dirichlet processes to create probability statements of any difference $\mathbb{P}(\phi_i \neq \phi_j)$. Our definition adds flexibility through a difference threshold parameter ϵ and thus accounts for applications where researchers have differing standards for what constitutes a disparity or are only interested in relatively large differences between random effects. Second, amongst other methods that consider differences in the spatial random effects with a continuous posterior distribution, our analysis framework uniquely stabilizes the difference probabilities with respect to the difference threshold ϵ . As a result, researchers can produce, say, a list of the top fifty disparities between neighboring counties knowing that the list will not change significantly if a different threshold is chosen.

Further steps to expand our approach could include applying a similar inference framework under a non-normal outcome, or formulating a reasonable framework for selecting an appropriate value of ρ to condition on in the exact conjugate model, which would enforce the aforementioned stability in the rankings of the posterior boundary probabilities. One could also consider modifying the definition of a difference boundary and apply a similar analysis framework to the posterior predictive distribution. We define difference probabilities on the modeled response level in Section S3 and prove ranking stability in the exact conjugate model. This leads to highly interpretable posterior difference probabilities on the response level, although it would arguably be less of a "spatial" disparity because the covariates are more closely intertwined with the predictive distribution.

7. SUPPLEMENTARY MATERIALS

Supplementary materials contains additional analysis on the behavior of the DIC and WAIC as $\rho \rightarrow 1^-$, formulation of an ϵ -difference probability on the modeled response level, and the full list of spatial disparities in the data analysis example. All computer programs required to reproduce the simulation and data analysis in this manuscript are available at https://github.com/Ky-Wu/bayesian_spatial_health_disparities.

REFERENCES

L. Aiello and S. Banerjee. Detecting spatial health disparities using disease maps, 2023. URL <https://arxiv.org/abs/2309.02086>.

- S. Banerjee. Modeling massive spatial datasets using a conjugate Bayesian linear modeling framework. *Spatial Statistics*, 37:100417, June 2020. ISSN 2211-6753. doi: 10.1016/j.spasta.2020.100417.
- S. Banerjee, B. P. Carlin, and A. E. Gelfand. *Hierarchical Modeling and Analysis for Spatial Data*. Number 135 in Monographs on Statistics and Applied Probability. CRC Press, Taylor & Francis Group, Boca Raton, second edition, 2015. ISBN 978-1-4398-1917-3.
- Y. Benjamini and Y. Hochberg. Controlling the False Discovery Rate: A Practical and Powerful Approach to Multiple Testing. *Journal of the Royal Statistical Society: Series B (Methodological)*, 57(1):289–300, 1995. ISSN 2517-6161. doi: 10.1111/j.2517-6161.1995.tb02031.x.
- J. Besag, J. York, and A. Mollié. Bayesian image restoration, with two applications in spatial statistics. *Annals of the Institute of Statistical Mathematics*, 43(1):1–20, Mar. 1991. ISSN 1572-9052. doi: 10.1007/BF00116466.
- F. Corpas-Burgos and M. A. Martínez-Beneito. On the use of adaptive spatial weight matrices from disease mapping multivariate analyses. *Stochastic Environmental Research and Risk Assessment*, 34:531–544, 2020.
- L. Dwyer-Lindgren, A. H. Mokdad, T. Srebotnjak, A. D. Flaxman, G. M. Hansen, and C. J. Murray. Cigarette smoking prevalence in US counties: 1996-2012. *Population Health Metrics*, 12(1):5, Mar. 2014. ISSN 1478-7954. doi: 10.1186/1478-7954-12-5.
- M. C. Fitzpatrick, E. L. Preisser, A. Porter, J. Elkinton, L. A. Waller, B. P. Carlin, and A. M. Ellison. Ecological boundary detection using bayesian areal wombling. *Ecology*, 91(12):3448–3455, 2010a. doi: <https://doi.org/10.1890/10-0807.1>. URL <https://esajournals.onlinelibrary.wiley.com/doi/abs/10.1890/10-0807.1>.
- M. C. Fitzpatrick, E. L. Preisser, A. Porter, J. Elkinton, L. A. Waller, B. P. Carlin, and A. M. Ellison. Ecological boundary detection using Bayesian areal wombling. *Ecology*, 91(12):3448–3514, Dec. 2010b. ISSN 0012-9658.
- L. Gao, S. Banerjee, and B. Ritz. Spatial Difference Boundary Detection for Multiple Outcomes Using Bayesian Disease Mapping. *Biostatistics*, 24(4):922–944, Oct. 2023. ISSN 1465-4644. doi: 10.1093/biostatistics/kxac013.
- A. Gelman. Prior distributions for variance parameters in hierarchical models (comment on article by Browne and Draper). *Bayesian Analysis*, 1(3):515–534, Sept. 2006. ISSN 1936-0975, 1931-6690. doi: 10.1214/06-BA117A.
- A. Gelman, J. Hwang, and A. Vehtari. Understanding predictive information criteria for Bayesian models. *Statistics and Computing*, 24(6):997–1016, Nov. 2014. ISSN 1573-1375. doi: 10.1007/s11222-013-9416-2.
- T. Hanson, S. Banerjee, P. Li, and A. McBean. Spatial boundary detection for areal counts. In *Nonparametric Bayesian Inference in Biostatistics*, pages 377–399. Springer, 2015.
- G. M. Jacquez and D. A. Greiling. Geographic boundaries in breast, lung and colorectal cancers in relation to exposure to air toxics in long island, new york. *International Journal of Health*

- Geographics*, 2(1):1–22, 2003a.
- G. M. Jacques and D. A. Greiling. Local clustering in breast, lung and colorectal cancer in long island, new york. *International Journal of Health Geographics*, 2(1):1–12, 2003b.
- E. T. Jaynes. Information Theory and Statistical Mechanics. *Physical Review*, 106(4):620–630, May 1957. ISSN 0031-899X. doi: 10.1103/PhysRev.106.620.
- A. B. Lawson. *Statistical methods in spatial epidemiology*. John Wiley & Sons, 2013.
- B. Lawson, Andrew, S. Banerjee, R. Haining, and D. Ugarte, Maria. *Handbook of Spatial Epidemiology*. CRC press, Boca Raton, FL, 2016.
- D. Lee and R. Mitchell. Boundary detection in disease mapping studies. *Biostatistics*, 13(3): 415–426, July 2012. ISSN 1465-4644. doi: 10.1093/biostatistics/kxr036.
- P. Li, S. Banerjee, and A. M. McBean. Mining boundary effects in areally referenced spatial data using the bayesian information criterion. *Geoinformatica*, 15(3):435–454, 2011.
- P. Li, S. Banerjee, B. P. Carlin, and A. M. McBean. Bayesian areal wombling using false discovery rates. *Statistics and its Interface*, 5(2):149–158, 2012.
- P. Li, S. Banerjee, T. A. Hanson, and A. M. McBean. Bayesian models for detecting difference boundaries in areal data. *Statistica Sinica*, 25(1):385, 2015.
- H. Lu and B. P. Carlin. Bayesian areal wombling for geographical boundary analysis. *Geographical Analysis*, 37(3):265–285, 2005.
- H. Lu, C. S. Reilly, S. Banerjee, and B. P. Carlin. Bayesian areal wombling via adjacency modeling. *Environmental and ecological statistics*, 14:433–452, 2007.
- H. Ma and B. P. Carlin. Bayesian multivariate areal wombling for multiple disease boundary analysis. *Bayesian Analysis*, 2(2):281–302, 2007.
- H. Ma, B. P. Carlin, and S. Banerjee. Hierarchical and joint site-edge methods for medicare hospice service region boundary analysis. *Biometrics*, 66(2):355–364, 2010.
- Z. Ma and G. Chen. Bayesian methods for dealing with missing data problems. *Journal of the Korean Statistical Society*, 47(3):297–313, Sept. 2018. ISSN 2005-2863. doi: 10.1016/j.jkss.2018.03.002.
- T. J. Mitchell and J. J. Beauchamp. Bayesian Variable Selection in Linear Regression. *Journal of the American Statistical Association*, 83(404):1023–1032, Dec. 1988. ISSN 0162-1459. doi: 10.1080/01621459.1988.10478694.
- A. H. Mokdad, L. Dwyer-Lindgren, C. Fitzmaurice, R. W. Stubbs, A. Bertozzi-Villa, C. Morozoff, R. Charara, C. Allen, M. Naghavi, and C. J. L. Murray. Trends and Patterns of Disparities in Cancer Mortality Among US Counties, 1980-2014. *JAMA*, 317(4):388–406, Jan. 2017. ISSN 0098-7484. doi: 10.1001/jama.2016.20324.
- P. Müller, G. Parmigiani, C. Robert, and J. Rousseau. Optimal Sample Size for Multiple Testing. *Journal of the American Statistical Association*, 99(468):990–1001, Dec. 2004. ISSN 0162-1459. doi: 10.1198/016214504000001646.

- P. Müller, G. Parmigiani, and K. Rice. FDR and Bayesian Multiple Comparisons Rules. In *Bayesian Statistics 8: Proceedings of the Eighth Valencia International Meeting June 2–6, 2006*. Oxford University Press, July 2007. ISBN 978-0-19-921465-5. doi: 10.1093/oso/9780199214655.003.0014.
- J. S. Rao. *Statistical Methods in Health Disparity Research*. Chapman & Hall/CRC, Boca Raton, FL, 2023.
- A. Riebler, S. H. Sørbye, D. Simpson, and H. Rue. An intuitive Bayesian spatial model for disease mapping that accounts for scaling. *Statistical Methods in Medical Research*, 25(4):1145–1165, Aug. 2016. ISSN 0962-2802. doi: 10.1177/0962280216660421.
- D. B. Rubin. Inference and missing data. *Biometrika*, 63(3):581–592, Dec. 1976. ISSN 0006-3444. doi: 10.1093/biomet/63.3.581.
- J. G. Scott and J. O. Berger. An exploration of aspects of Bayesian multiple testing. *Journal of Statistical Planning and Inference*, 136(7):2144–2162, July 2006. ISSN 0378-3758. doi: 10.1016/j.jspi.2005.08.031.
- G. A. Seber and A. J. Lee. Hypothesis Testing. In *Linear Regression Analysis*, chapter 4, pages 97–118. John Wiley & Sons, Ltd, 2003. ISBN 978-0-471-72219-9. doi: 10.1002/9780471722199.ch4.
- C. E. Shannon. A Mathematical Theory of Communication. *Bell System Technical Journal*, 27(3): 379–423, July 1948. ISSN 00058580. doi: 10.1002/j.1538-7305.1948.tb01338.x.
- A. H. Shreves, I. D. Buller, E. Chase, H. Creutzfeldt, J. A. Fisher, B. I. Graubard, R. N. Hoover, D. T. Silverman, S. S. Devesa, and R. R. Jones. Geographic Patterns in U.S. Lung Cancer Mortality and Cigarette Smoking. *Cancer Epidemiology, Biomarkers & Prevention*, 32(2):193–201, Feb. 2023. ISSN 1055-9965. doi: 10.1158/1055-9965.EPI-22-0253.
- D. Simpson, H. Rue, A. Riebler, T. G. Martins, and S. H. Sørbye. Penalising Model Component Complexity: A Principled, Practical Approach to Constructing Priors. *Statistical Science*, 32(1): 1–28, 2017. ISSN 0883-4237.
- D. J. Spiegelhalter, N. G. Best, B. P. Carlin, and A. Van Der Linde. Bayesian measures of model complexity and fit. *Journal of the Royal Statistical Society: Series B (Statistical Methodology)*, 64(4):583–639, 2002. ISSN 1467-9868. doi: 10.1111/1467-9868.00353.
- L. Waller and B. Carlin. Disease mapping. In A. E. Gelfand, P. Diggle, P. Guttorp, and M. Fuentes, editors, *Handbook Of Spatial Statistics*, page 217–243. CRC Press, Boca Raton, FL, 2010.
- L. A. Waller and C. A. Gotway. *Applied spatial statistics for public health data*, volume 368. John Wiley & Sons, 2004.
- S. Watanabe. Asymptotic Equivalence of Bayes Cross Validation and Widely Applicable Information Criterion in Singular Learning Theory. *Journal of Machine Learning Research*, 11(116): 3571–3594, 2010. ISSN 1533-7928.

APPENDIX A. PROOF OF THEOREM 1

Under the settings of Theorem 1, we will show that $p_k > p_{k'}$ if and only if $v_k(\epsilon) < v_{k'}(\epsilon)$.

Proof. Under the standard linear model described in Theorem 1, the p-values, $p_k = \mathbb{P}\left(t > |t_{\text{obs}}^{(k)}|\right)$, are characterized by a common t-distribution CDF evaluated at the observed t-statistics. As CDFs are monotonic functions, $p_k > p_{k'}$ if and only if $|t_{\text{obs}}^{(k)}| < |t_{\text{obs}}^{(k')}|$. Next, it is well known that when $\pi(\beta, \sigma^2) \propto \pi(\sigma^2)$, then $\beta | y, \sigma^2 \sim N\left(\widehat{\beta}, \sigma^2(X^T V_y^{-1} X)^{-1}\right)$, where $\widehat{\beta} = (X^T V_y^{-1} X)^{-1} X^T V_y^{-1} y$ is the generalized least squares estimate. We have that for any $\epsilon > 0, \sigma^2 > 0$,

$$\begin{aligned} \mathbb{P}\left(\frac{|c_k^T \beta|}{\sigma \sqrt{c_k^T M c_k}} > \epsilon \mid y, \sigma^2\right) &= 1 - \mathbb{P}\left(-\epsilon \leq \frac{c_k^T \beta}{\sigma \sqrt{c_k^T (X^T V_y^{-1} X)^{-1} c_k}} \leq \epsilon \mid y, \sigma^2\right) \\ &= \Phi\left(-\epsilon + \frac{c_k^T \widehat{\beta}}{\sigma \sqrt{c_k^T (X^T V_y^{-1} X)^{-1} c_k}}\right) + \Phi\left(-\epsilon - \frac{c_k^T \widehat{\beta}}{\sigma \sqrt{c_k^T (X^T V_y^{-1} X)^{-1} c_k}}\right) \\ &= \Phi\left(-\epsilon + \frac{\widehat{\sigma}}{\sigma} t_{\text{obs}}^{(k)}\right) + \Phi\left(-\epsilon - \frac{\widehat{\sigma}}{\sigma} t_{\text{obs}}^{(k)}\right) \end{aligned}$$

where Φ denotes the standard normal CDF. Let $h_c : \mathbb{R} \rightarrow [0, 1]$ be given by $h_c(x) = \Phi(-\epsilon + cx) + \Phi(-\epsilon - cx)$ for some $c > 0$. Then, $h'_c(x) = c f_Z(-\epsilon + cx) - c f_Z(-\epsilon - cx)$, where f_Z is the standard normal density. Since $\epsilon > 0, c > 0$, and f_Z is centered around 0, then $h'_c(x) > 0$ for $x > 0$, and $h'_c(x) < 0$ for $x < 0$. If $x, y \in \mathbb{R}$, then $h_c(x) = h_c(-x)$ and $|x| > |y|$ if and only if $h_c(-x) = h_c(x) > h_c(y) = h_c(-y)$. Since $c > 0$ was arbitrary,

$$|t_{\text{obs}}^{(k)}| < |t_{\text{obs}}^{(k')}| \iff \mathbb{P}\left(\frac{|c_k^T \beta|}{\sigma \sqrt{c_k^T M c_k}} > \epsilon \mid y, \sigma^2\right) < \mathbb{P}\left(\frac{|c_{k'}^T \beta|}{\sigma \sqrt{c_{k'}^T M c_{k'}}} > \epsilon \mid y, \sigma^2\right)$$

for any $\epsilon > 0, \sigma^2 > 0$. Marginalizing out σ^2 preserves the order as

$$\begin{aligned} v_k(\epsilon) &= \mathbb{P}\left(\frac{|c_k^T \beta|}{\sigma \sqrt{c_k^T M c_k}} > \epsilon \mid y\right) = \int_0^\infty \mathbb{P}\left(\frac{|c_k^T \beta|}{\sigma \sqrt{c_k^T M c_k}} > \epsilon \mid y, \sigma^2\right) \pi(\sigma^2 | y) d\sigma^2 \\ &< \int_0^\infty \mathbb{P}\left(\frac{|c_{k'}^T \beta|}{\sigma \sqrt{c_{k'}^T M c_{k'}}} > \epsilon \mid y, \sigma^2\right) \pi(\sigma^2 | y) d\sigma^2 \\ &= \mathbb{P}\left(\frac{|c_{k'}^T \beta|}{\sigma \sqrt{c_{k'}^T M c_{k'}}} > \epsilon \mid y\right) = v_{k'}(\epsilon) \end{aligned}$$

which shows that $\left|t_{\text{obs}}^{(k)}\right| < \left|t_{\text{obs}}^{(k')}\right|$ implies $v_k(\epsilon) < v_{k'}(\epsilon)$ for all $\epsilon > 0$. If $v_k(\epsilon) < v_{k'}(\epsilon)$ for all $\epsilon > 0$, then this implies there exists $\epsilon > 0, \sigma^2 > 0$ such that $\mathbb{P}\left(\frac{|c_k^T \beta|}{\sigma \sqrt{c_k^T M c_k}} > \epsilon \mid y, \sigma^2\right) < \mathbb{P}\left(\frac{|c_{k'}^T \beta|}{\sigma \sqrt{c_{k'}^T M c_{k'}}} > \epsilon \mid y, \sigma^2\right)$, which implies $\left|t_{\text{obs}}^{(k)}\right| < \left|t_{\text{obs}}^{(k')}\right|$ by the above argument. Therefore, we have shown

$$\begin{aligned} p_k > p_{k'} &\iff \left|t_{\text{obs}}^{(k)}\right| < \left|t_{\text{obs}}^{(k')}\right| \\ &\iff \mathbb{P}\left(\frac{|c_k^T \beta|}{\sigma \sqrt{c_k^T M c_k}} > \epsilon \mid y, \sigma^2\right) < \mathbb{P}\left(\frac{|c_{k'}^T \beta|}{\sigma \sqrt{c_{k'}^T M c_{k'}}} > \epsilon \mid y, \sigma^2\right) \forall \sigma^2, \epsilon > 0 \\ &\iff v_k(\epsilon) < v_{k'}(\epsilon) \forall \epsilon > 0 \end{aligned}$$

completing the proof.

APPENDIX B. PROOF OF THEOREM 2

Under the settings of Theorem 2, we will show that if there exists $\epsilon_\star > 0$ such that $h_k(\epsilon_\star; \rho) < h_{k'}(\epsilon_\star; \rho)$, then $h_k(\epsilon; \rho) < h_{k'}(\epsilon; \rho)$ for all $\epsilon > 0$.

Proof. The posterior conditional distributions from the augmented linear system in (5) are given by (6) so $\gamma_\star \mid y, \rho, \sigma^2 \sim N_{n+p}(M_\star m_\star, \sigma^2 M_\star)$. For all $k = 1, \dots, K$, denote $\alpha_k = \frac{c_k^T M_\star m_\star}{\sqrt{c_k^T (X_\star^T V_{y_\star}^{-1} X_\star)^{-1} c_k}}$.

For any $0 < \rho < 1$,

$$\begin{aligned} \mathbb{P}\left(\frac{|c_k^T \gamma_\star|}{\sigma \sqrt{c_k^T (X_\star^T V_{y_\star}^{-1} X_\star)^{-1} c_k}} > \epsilon \mid y, \rho, \sigma^2\right) &= 1 - \mathbb{P}\left(-\epsilon \leq \frac{c_k^T \gamma_\star}{\sigma \sqrt{c_k^T (X_\star^T V_{y_\star}^{-1} X_\star)^{-1} c_k}} \leq \epsilon \mid y, \rho, \sigma^2\right) \\ &= \Phi\left(-\epsilon + \frac{\alpha_k}{\sigma}\right) + \Phi\left(-\epsilon - \frac{\alpha_k}{\sigma}\right) \end{aligned}$$

By the analysis in Appendix A, this implies that for any $k \neq k'$, $|\alpha_k| < |\alpha_{k'}|$ if and only if $\mathbb{P}\left(\frac{|c_k^T \gamma_\star|}{\sigma \sqrt{c_k^T (X_\star^T V_{y_\star}^{-1} X_\star)^{-1} c_k}} > \epsilon \mid y, \rho, \sigma^2\right) < \mathbb{P}\left(\frac{|c_{k'}^T \gamma_\star|}{\sigma \sqrt{c_{k'}^T (X_\star^T V_{y_\star}^{-1} X_\star)^{-1} c_{k'}}} > \epsilon \mid y, \rho, \sigma^2\right)$ for all $\sigma^2 > 0, \epsilon > 0$. Thus, if there exists $\epsilon_\star > 0$ such that $h_k(\epsilon_\star; \rho) < h_{k'}(\epsilon_\star; \rho)$, then this means that there exists

$\sigma^2 > 0$ such that $\mathbb{P}\left(\frac{|c_k^T \gamma_\star|}{\sigma \sqrt{c_k^T (X_\star^T V_{y_\star}^{-1} X_\star)^{-1} c_k}} > \epsilon_\star \mid y, \rho, \sigma^2\right) < \mathbb{P}\left(\frac{|c_{k'}^T \gamma_\star|}{\sigma \sqrt{c_{k'}^T (X_\star^T V_{y_\star}^{-1} X_\star)^{-1} c_{k'}}} > \epsilon_\star \mid y, \rho, \sigma^2\right)$,

which implies $|\alpha_k| < |\alpha_{k'}|$. Thus, for any $\epsilon > 0$,

$$\begin{aligned}
h_k(\epsilon; \rho) &= \int_0^\infty \mathbb{P} \left(\frac{|c_k^\top \gamma_\star|}{\sigma \sqrt{c_k^\top (X_\star^\top V_{y_\star}^{-1} X_\star)^{-1} c_k}} > \epsilon \mid y, \rho, \sigma^2 \right) \pi(\sigma^2 \mid y, \rho) d\sigma^2 \\
&< \int_0^\infty \mathbb{P} \left(\frac{|c_{k'}^\top \gamma_\star|}{\sigma \sqrt{c_{k'}^\top (X_\star^\top V_{y_\star}^{-1} X_\star)^{-1} c_{k'}}} > \epsilon \mid y, \rho, \sigma^2 \right) \pi(\sigma^2 \mid y, \rho) d\sigma^2 \\
&= h_{k'}(\epsilon; \rho)
\end{aligned}$$

which completes the proof.

**SUPPLEMENTARY MATERIAL FOR ASSESSING SPATIAL DISPARITIES: A
BAYESIAN LINEAR REGRESSION APPROACH**

KYLE LIN WU AND SUDIPTO BANERJEE

S1. BEHAVIOR OF DIC IN SELECTING ρ IN EXACT MODEL

In our simulations, the DIC and WAIC always suggest picking ρ arbitrarily close to 1. We show analytically that the DIC diverges to $-\infty$ as $\rho \rightarrow 1^-$.

Suppose that under the model given by (4), the prior is $\pi(\beta, \gamma, \sigma^2) = N(\gamma | 0, \sigma^2 \rho V_\phi) \times \text{IG}(\sigma^2 | a_{\sigma^2}, b_{\sigma^2})$ and consider the modeled response $Y | \beta, \gamma, \sigma^2, \rho \sim N(X\beta + \gamma, \sigma^2(1 - \rho))$. Assume $0 \leq \rho \leq 1$ and positive definite V_ϕ^{-1} are known. Denote $\gamma_\star = (\beta^\top, \gamma^\top)^\top$. Then, by the theory provided by casting to an augmented linear system, $\gamma_\star | y, \sigma^2, \rho \sim N(M_\star m_\star, \sigma^2 M_\star)$ and $\sigma^2 | y, \rho \sim \text{IG}(a_n, b_n)$ where $a_n = a_{\sigma^2} + \frac{n}{2}$, $b_n = b_{\sigma^2} + \frac{1}{2} \left(\frac{y^\top y}{1-\rho} - m_\star^\top M_\star m_\star \right)$, $M_\star = \left(X_\star^\top V_{y_\star}^{-1} X_\star \right)^{-1}$, and $m_\star = X_\star^\top V_{y_\star}^{-1} y_\star = \left(\frac{1}{1-\rho} X^\top y, \frac{1}{1-\rho} y \right)^\top$.

The posterior means are given by $\hat{\gamma}_\star = M_\star m_\star$, $\hat{\sigma}^2 = \frac{b_n}{a_n - 1}$. Let $\theta = (\beta, \gamma, \sigma^2)^\top$, $W = \begin{bmatrix} X & I_n \end{bmatrix}$. Then, $\text{DIC}(\rho) = -2 \log p(y | \hat{\theta}) + 2p_{\text{DIC}}$ where

$$\begin{aligned} \log p(y | \theta) &= -\frac{n}{2} \log(2\pi(1-\rho)) - \frac{n}{2} \log(\sigma^2) - \frac{(y - W\gamma_\star)^\top (y - W\gamma_\star)}{2\sigma^2(1-\rho)} \\ \log p(y | \hat{\theta}) &= -\frac{n}{2} \log(2\pi(1-\rho)) - \frac{n}{2} \log\left(\frac{b_n}{a_n - 1}\right) - \frac{(a_n - 1) \|y - WM_\star m_\star\|^2}{2b_1(1-\rho)} \\ \mathbb{E}_{\theta|y} [\log p(y | \theta)] &= -\frac{n}{2} \log(2\pi(1-\rho)) + \frac{n}{2} (\psi(a_n) - \log(b_n)) - \frac{\text{tr}(WM_\star W^\top)}{2(1-\rho)} - \frac{a_n \|y - WM_\star m_\star\|^2}{2b_1(1-\rho)} \\ p_{\text{DIC}} &= \frac{n}{2} (\log(a_n - 1) - \psi(a_n)) + \frac{\text{tr}(WM_\star W^\top)}{2(1-\rho)} + \frac{\|y - WM_\star m_\star\|^2}{2b_1(1-\rho)} \end{aligned}$$

where $\psi(x)$ is the digamma function. We now show that $\lim_{\rho \rightarrow 1^-} b_n(\rho) < \infty$. Denote $B = \frac{1-\rho}{\rho} V_\phi^{-1} + I_n - H$. By the theory of the augmented linear system, $b_n = b_{\sigma^2} + \frac{1}{2(1-\rho)} (y^\top (I_n - H)y - e^\top B^{-1}e)$, where $\frac{1}{2(1-\rho)} (y^\top (I_n - H)y - e^\top B^{-1}e) = \frac{1}{2(1-\rho)} e^\top (I - B^{-1})e$. By spectral decomposition, $V_\phi^{1/2} (I - H) V_\phi^{1/2} = CDC^\top$ where C is an orthogonal matrix and $D = \text{diag}(d_1, \dots, d_n)$ with entries that are the non-negative eigenvalues of $V_\phi^{1/2} (I - H) V_\phi^{1/2}$. Let $U = V_\phi^{1/2} C$, then U is invertible, $U^\top V_\phi^{-1} U = I_n$, $U^\top (I_n - H) U = D$, and $B^{-1} = U \left(D + \frac{1-\rho}{\rho} I_n \right)^{-1} U^\top$. Define $v = U^{-1}e$, then

Date: July 30, 2024.

$e^\top B^{-1}e = v^\top D \left(D + \frac{1-\rho}{\rho} I_n \right)^{-1} Dv$ and

$$\begin{aligned}
\lim_{\rho \rightarrow 1^-} b_n &= \lim_{\rho \rightarrow 1^-} b_{\sigma^2} + \frac{1}{2(1-\rho)} e^\top (I - B^{-1})e \\
&= b_{\sigma^2} + \lim_{\rho \rightarrow 1^-} \frac{1}{2(1-\rho)} \left(v^\top Dv - v^\top D \left(D + \frac{1-\rho}{\rho} I_n \right)^{-1} Dv \right) \\
&= b_{\sigma^2} + \lim_{\rho \rightarrow 1^-} \frac{\sum_{d_j \neq 0} \left(v_j^2 d_j - \frac{v_j^2 d_j^2}{d_j + \frac{1-\rho}{\rho}} \right)}{2(1-\rho)} \\
&= b_{\sigma^2} + \lim_{\rho \rightarrow 1^-} \sum_{d_j \neq 0} \left(\frac{v_j^2 d_j^2}{2\rho^2 \left(d_j + \frac{1-\rho}{\rho} \right)^2} \right) = b_{\sigma^2} + \sum_{d_j \neq 0} \frac{v_j^2}{2} < \infty
\end{aligned}$$

where the second to last equality follows from L'Hôpital's Rule. Denote $b = \lim_{\rho \rightarrow 1^-} b_n(\rho) = b_{\sigma^2} + \sum_{d_j \neq 0} \frac{v_j^2}{2}$. We next show that $\lim_{\rho \rightarrow 1^-} \frac{\|y - WM_\star m_\star\|^2}{1-\rho} = 0$. By the theory of the augmented linear system, $y - W\hat{\gamma}_\star = (I_n - H)(I - B^{-1})e$ where $H = X(X^\top X)^{-1}X^\top$. Further evaluation yields $\|y - WM_\star m_\star\|^2 = e^\top (I_n - H - 2B^{-1} - 2B^{-1} + B^{-1}(I_n - H)B^{-1})e$. Letting $v = U^{-1}e$ again, we obtain $\frac{\|y - WM_\star m_\star\|^2}{1-\rho} = v^\top \left(D - 2D \left[D + D^2 \frac{1-\rho}{\rho} I_n \right]^{-1} + D^3 \left[D + \frac{1-\rho}{\rho} I_n \right]^{-2} \right) v$ and

$$\begin{aligned}
\lim_{\rho \rightarrow 1^-} \frac{\|y - WM_\star m_\star\|^2}{1-\rho} &= \lim_{\rho \rightarrow 1^-} \sum_{d_j \neq 0} \frac{v_j^2}{1-\rho} \left(d_j - 2 \frac{d_j^2}{d_j + \frac{1-\rho}{\rho}} + \frac{d_j^3}{\left(d_j + \frac{1-\rho}{\rho} \right)^2} \right) \\
&= - \lim_{\rho \rightarrow 1^-} \sum_{d_j \neq 0} v_j^2 \left(-2 \frac{d_j^2}{\left(d_j + \frac{1-\rho}{\rho} \right)^2 \rho^2} + \frac{2d_j^3}{\left(d_j + \frac{1-\rho}{\rho} \right)^3 \rho^2} \right)
\end{aligned}$$

which can be evaluated to give the result $\lim_{\rho \rightarrow 1^-} \frac{\|y - WM_\star m_\star\|^2}{1-\rho} = 0$. Next, evaluating the expression $\frac{W^\top WM_\star}{1-\rho}$ yields $\frac{\text{tr}(WM_\star W^\top)}{1-\rho} = p + \text{tr}((I_n - H)B^{-1})$. Furthermore,

$$\begin{aligned}
\lim_{\rho \rightarrow 1^-} \text{tr} \left((I_n - H)B^{-1} \right) &= \lim_{\rho \rightarrow 1^-} \text{tr} \left((I_n - H)U \left(D + \frac{1-\rho}{\rho} I_n \right)^{-1} U^\top \right) \\
&= \lim_{\rho \rightarrow 1^-} \text{tr} \left(D \left(D + \frac{1-\rho}{\rho} I_n \right)^{-1} \right) \\
&= \lim_{\rho \rightarrow 1^-} \sum_{d_j \neq 0} \frac{d_j}{d_j + \frac{1-\rho}{\rho}} \\
&= \sum_{d_j \neq 0} 1 = \text{tr}(I_n - H) = n - p
\end{aligned}$$

Therefore, $\lim_{\rho \rightarrow 1^-} \frac{\text{tr}(WM_\star W^T)}{1-\rho} = n$. Combining our previous results, we have shown that

$$\lim_{\rho \rightarrow 1^-} p_{DIC} = \lim_{\rho \rightarrow 1^-} 2 \left(\log p(y|\hat{\theta}) - \mathbb{E}_{\theta|y} [\log p(y|\theta)] \right) = n + n(\log(a_n - 1) - \psi(a_n))$$

This is an intuitive result because p_{DIC} represents the number of effective parameters in the model and if n is large enough, a_{σ^2} small enough, then $\lim_{\rho \rightarrow 1^-} p_{DIC} \approx n + 1$, which penalizes heavy overfitting through the n spatial residuals. However, we have also shown that every term in $\log p(y|\hat{\theta})$ converges except $-\frac{n}{2} \log(2\pi(1-\rho))$, which diverges to ∞ as ρ becomes arbitrarily close to 1. Therefore, this shows that $\lim_{\rho \rightarrow 1^-} \text{DIC}(\rho) = \lim_{\rho \rightarrow 1^-} (-2 \log p(y|\hat{\theta}) + 2p_{DIC}) = -\infty$.

S2. BEHAVIOR OF WAIC IN SELECTING ρ IN EXACT MODEL

We sketch out an argument for the behavior of WAIC as ρ grows arbitrarily close to 1 in the exact model. Similar to the computation for the DIC, it can be shown that $\lim_{\rho \rightarrow 1^-} p_{WAIC2} < \infty$, so it suffices to show that $\lim_{\rho \rightarrow 1^-} \text{lppd}(\rho) = \sum_{i=1}^n \lim_{\rho \rightarrow 1^-} \log(p_{\text{post}}(y_i)) = \infty$.

We again consider the model given by (4), where the prior is $\pi(\beta, \gamma, \sigma^2) = N(\gamma | 0, \sigma^2 \rho V_\phi) \times \text{IG}(\sigma^2 | a_{\sigma^2}, b_{\sigma^2})$ and the modeled response $Y | \beta, \gamma, \sigma^2, \rho \sim N(X\beta + \gamma, \sigma^2(1-\rho))$ where we assume $0 \leq \rho \leq 1$ and V_ϕ is positive definite are known. Let $W = \begin{bmatrix} X & I_n \end{bmatrix}$, then

$$\begin{aligned} p_{\text{post}}(Y | \sigma^2, \rho) &\propto \int_{\gamma_\star} \exp \left(-\frac{(Y - W\gamma_\star)^T (Y - W\gamma_\star)}{2\sigma^2(1-\rho)} - \frac{(\gamma_\star - M_\star m_\star)^T M_\star^{-1} (\gamma_\star - M_\star m_\star)}{2\sigma^2} \right) d\gamma_\star \\ &\propto \exp \left(-\frac{Y^T Y}{2\sigma^2(1-\rho)} - \frac{\left(\frac{1}{1-\rho} W^T Y + m_\star \right)^T \left(\frac{W^T W}{1-\rho} + M_\star^{-1} \right)^{-1} \left(\frac{1}{1-\rho} W^T Y + m_\star \right)}{2\sigma^2} \right) \end{aligned}$$

Let $V_1 = W^T W + (1-\rho)M_\star^{-1}$, then since $m_\star = \frac{1}{1-\rho} W^T y$, this simplifies to

$$\begin{aligned} p_{\text{post}}(Y | \sigma^2, \rho) &\propto \exp \left(\frac{Y^T Y - (Y + y)^T W V_1^{-1} W^T (Y + y)}{2\sigma^2(1-\rho)} \right) \\ &\propto \exp \left(\frac{Y^T (I_n - W V_1^{-1} W^T) Y - 2Y^T W V_1^{-1} W^T y}{2\sigma^2(1-\rho)} \right) \end{aligned}$$

Hence, $Y | y, \sigma^2, \rho \sim N_n \left((I_n - W V_1^{-1} W^T)^{-1} W V_1^{-1} W^T y, \sigma^2(1-\rho) (I_n - W V_1^{-1} W^T)^{-1} \right)$. Using the

theory of the augmented linear system, we can evaluate $V_1 = \begin{bmatrix} 2X^T X & 2X^T \\ 2X & 2I_n + \frac{1-\rho}{\rho} V_\phi^{-1} \end{bmatrix}$. Denoting

$H = X(X^T X)^{-1} X^T$, $B = (I_n - H) + \frac{1-\rho}{\rho} V_\phi^{-1}$, we have $W V_1^{-1} W^T = \frac{1}{2} H + (I_n - H)(B + I_n - H)^{-1}(I_n - H)$.

By spectral decomposition, $V_\phi^{1/2}(I - H)V_\phi^{1/2} = CDC^T$ where C is an orthogonal matrix and $D = \text{diag}(d_1, \dots, d_n)$ with entries that are the non-negative eigenvalues of $V_\phi^{1/2}(I - H)V_\phi^{1/2}$. Let

$U = V_\phi^{1/2} C$, then U is invertible, $U^T V_\phi^{-1} U = I_n$, $U^T (I_n - H) U = D$, and $B^{-1} = U \left(D + \frac{1-\rho}{\rho} I_n \right)^{-1} U^T$.

Thus,

$$\begin{aligned}
I_n - WV_1^{-1}W^T &= I_n - \frac{1}{2}H - (I_n - H)(B + I_n - H)^{-1}(I_n - H) \\
&= I_n - \frac{1}{2}H - U^{-T}DU^{-1} \left(2U^{-T}DU^{-1} + \frac{1-\rho}{\rho}U^{-T}U^{-1} \right)^{-1} U^{-T}DU^{-1} \\
&= I_n - \frac{1}{2}H - U^{-T}D \left(2D + \frac{1-\rho}{\rho}I_n \right)^{-1} DU^{-1}
\end{aligned}$$

Let $W = D \left(2D + \frac{1-\rho}{\rho}I_n \right)^{-1} D$, then $W_{ii} = \frac{d_i^2}{2d_i + \frac{1-\rho}{\rho}}$. If $d_j = 0$, then $W_{jj} = 0$. Thus, $\lim_{\rho \rightarrow 1^-} W = \frac{1}{2}D$. Hence,

$$\lim_{\rho \rightarrow 1^-} (I - WV_1^{-1}W^T) = I - \frac{1}{2}H - \frac{1}{2}U^{-T}DU^{-1} = I - \frac{1}{2}H - \frac{1}{2}(I_n - H) = \frac{1}{2}I$$

which also implies $\lim_{\rho \rightarrow 1^-} (I_n - WV_1^{-1}W^T)^{-1} WV_1^{-1}W^T = I_n$. Define $Z = \frac{Y-y}{\sqrt{2\sigma^2(1-\rho)}} \Big| y, \sigma^2, \rho$ with probability density function $f_{\text{post}}(z)$. The above result means that for all $z \in \mathbb{R}$, $\lim_{\rho \rightarrow 1^-} f_{\text{post}}(z) = f(z)$, where f denotes the standard normal CDF. That is, as ρ grows arbitrarily close to 1, the modeled response $Y | y, \sigma^2, \rho$ is asymptotically distributed as $N_n(y, 2\sigma^2(1-\rho)I_n)$. By this argument, $Y_i | y, \sigma^2, \rho$ is asymptotically distributed as $N(y_i | 2\sigma^2(1-\rho))$ when $\rho \rightarrow 1^-$ for $i = 1, \dots, n$. Denote the pdf of $Y_i | y, \sigma^2, \rho$ as $f_{Y_i}(y_i | \sigma^2, \rho)$, then this directly implies that $\lim_{\rho \rightarrow 1^-} \log(p_{\text{post}}(y_i)) = \lim_{\rho \rightarrow 1^-} \int_0^\infty f_{Y_i}(y_i | \sigma^2, \rho) \pi(\sigma^2 | y, \rho) d\sigma^2 = \infty$. Hence, $\lim_{\rho \rightarrow 1^-} \text{lppd}(\rho) = \infty$, so $\text{WAIC}(\rho) = -2\text{lppd} + 2p_{\text{WAIC}2}$ diverges to $-\infty$ as $\rho \rightarrow 1^-$.

S3. CONSTRUCTION OF DIFFERENCE PROBABILITIES ON MODELED RESPONSE LEVEL

To consider difference probabilities on the modeled response level, we begin with the exact model setting, where the modeled response $Y | \beta, \gamma, \sigma^2, \rho \sim N(X\beta + \gamma, \sigma^2(1-\rho))$ and the prior is $\pi(\beta, \gamma, \sigma^2) = N(\gamma | 0, \sigma^2\rho V_\phi) \times \text{IG}(\sigma^2 | a_{\sigma^2}, b_{\sigma^2})$. Since this is the exact model, we assume $0 \leq \rho \leq 1$ and positive definite V_ϕ are known. Denote $\gamma_\star = (\beta^T, \gamma^T)^T$.

Suppose now that we are interested in linear combinations of the modeled response $c_k^T Y$ where $c_1, \dots, c_K \in \mathbb{R}^n$ and $Y \sim N(X\beta + \gamma, \sigma^2(1-\rho))$ is the posterior predictive distribution. Let $\gamma_\star = (\beta, \gamma)^T$, and as discussed in Section 2.2, $\gamma_\star | \sigma^2, \rho \sim N(M_\star m_\star, \sigma^2 M_\star)$, $\sigma^2 | y, \rho \sim \text{IG}(a_n, b_n)$. Next, $Y | y, \sigma^2, \rho \sim N_n \left((I_n - WV_1^{-1}W^T)^{-1} WV_1^{-1}W^T y, \sigma^2(1-\rho) (I_n - WV_1^{-1}W^T)^{-1} \right)$ as shown in Section S2, where $WV_1^{-1}W^T = \frac{1}{2}H + (I_n - H)(B + I_n - H)^{-1}(I_n - H)$, $B = I_n - H + \frac{1-\rho}{\rho}V_\phi^{-1}$ and V_ϕ is assumed positive definite. For $\epsilon > 0$, define the conditional ϵ -difference probabilities as

$$h_k(\epsilon; \rho) = \mathbb{P} \left(\frac{|c_k^T Y| / \sqrt{\sigma^2(1-\rho)}}{\sqrt{c_k^T (I_n - WV_1^{-1}W^T)^{-1} c_k}} > \epsilon \Big| y, \rho \right)$$

for $k = 1, \dots, K$. Let $0 \neq c_i, c_j \in \mathbb{R}^n$ and set $\alpha_i = \frac{\mathbb{E}(c_i^T Y | y, \sigma^2, \rho)}{\sqrt{\text{Var}(c_i^T Y | y, \sigma^2, \rho)}} = \frac{c_i^T (I_n - W V_1^{-1} W^T)^{-1} W V_1^{-1} y}{\sqrt{(1-\rho) c_i^T (I_n - W V_1^{-1} W^T)^{-1} c_i}}$. We show that the rankings of these posterior probabilities are stable by proving that given two vectors $c_i, c_j \in \mathbb{R}^n, 0 < \rho < 1$, if the corresponding conditional probabilities satisfy $h_i(\epsilon; \rho) < h_j(\epsilon; \rho)$ for some $\epsilon > 0$, then $h_i(\epsilon; \rho) < h_j(\epsilon; \rho)$ for all $\epsilon > 0$. First, define

$$\begin{aligned} w_i(\epsilon; \sigma^2, \rho) &= \mathbb{P} \left(\frac{|c_i^T Y| / \sqrt{\sigma^2(1-\rho)}}{\sqrt{c_i^T (I_n - W V_1^{-1} W^T)^{-1} c_i}} > \epsilon \mid y, \sigma^2, \rho \right) \\ &= \mathbb{P} \left(-\epsilon - \frac{\alpha_i}{\sigma} \leq Z \leq \epsilon - \frac{\alpha_i}{\sigma} \right), \quad Z \sim N(0, 1) \\ &= \Phi \left(-\epsilon + \frac{\alpha_i}{\sigma} \right) + \Phi \left(-\epsilon - \frac{\alpha_i}{\sigma} \right) \end{aligned}$$

where Φ denotes the standard normal CDF. Let $f : \mathbb{R} \rightarrow \mathbb{R}$ be given by $f(x) = \Phi(-\epsilon + \frac{x}{\sigma}) + \Phi(-\epsilon - \frac{x}{\sigma})$ for any $\sigma > 0$. Then, as shown in the proof for the standard linear model case, for any $x, y \in \mathbb{R}, |x| > |y|$ if and only if $f(x) > f(y)$. Therefore, for any $\sigma^2 > 0, w_i(\epsilon; \sigma^2, \rho) > w_j(\epsilon; \sigma^2, \rho)$ if and only if $|\alpha_i(\sigma^2)| > |\alpha_j(\sigma^2)|$. Thus, if $|\alpha_i| > |\alpha_j|$, then

$$h_i(\epsilon; \rho) = \int_0^\infty w_i(\epsilon; \sigma^2, \rho) \pi(\sigma^2 | y) d\sigma^2 < \int_0^\infty w_j(\epsilon; \sigma^2, \rho) \pi(\sigma^2 | y) d\sigma^2 = h_j(\epsilon; \rho)$$

for all $\epsilon > 0$. Likewise, if $h_i(\epsilon; \rho) < h_j(\epsilon; \rho)$ for all ϵ , then there exists $\epsilon > 0, \sigma^2 > 0$ such that $w_i(\epsilon; \sigma^2, \rho) > w_j(\epsilon; \sigma^2, \rho)$ which implies $|\alpha_i| > |\alpha_j|$. Since the statement $|\alpha_i| > |\alpha_j|$ does not depend on ϵ , we conclude that if $h_i(\epsilon; \rho) < h_j(\epsilon; \rho)$ for some given $\epsilon > 0$, then $h_i(\epsilon; \rho) < h_j(\epsilon; \rho)$ for all $\epsilon > 0$.

Similar to the ϵ -difference probabilities on the effects level, one can define the corresponding marginal posterior ϵ -difference probabilities as

$$v_k(\epsilon) = \mathbb{P} \left(\frac{|c_k^T Y| / \sqrt{\sigma^2(1-\rho)}}{\sqrt{c_k^T (I_n - W V_1^{-1} W^T)^{-1} c_k}} > \epsilon \mid y \right)$$

for $0 \neq c_k \in \mathbb{R}^n$ and a joint prior $\pi(\beta, \gamma, \sigma^2, \rho)$.

S4. CLASSIFIED SPATIAL DISPARITIES IN COUNTY-LEVEL TRACHEAL, BRONCHUS, AND LUNG CANCER MORTALITY RATES

In Section 5, we apply the maximum conditional entropy criterion to select the difference threshold $\epsilon_{CE} = 0.845$ and set the Bayesian FDR tolerance at $\delta = 0.2$ to obtain 460 classified spatial difference boundaries out of 8,793 pairs of geographically adjacent counties within the

continental USA. The full list of disparities are shown in Table S1, along with Monte Carlo estimates of $v_k(\epsilon_{CE}) = \mathbb{P}\left(\frac{|a_k^T \phi|}{\sqrt{a_k^T \text{Var}(\phi|y,\rho)a_k}} > \epsilon \mid y\right)$.

	County 1	County 2	$v_k(\epsilon_{CE})$
1	Alachua County, Florida	Union County, Florida	1.000
2	Baker County, Florida	Union County, Florida	1.000
3	Bradford County, Florida	Union County, Florida	1.000
4	Columbia County, Florida	Union County, Florida	1.000
5	Boone County, Kentucky	Gallatin County, Kentucky	1.000
6	Clark County, Kentucky	Powell County, Kentucky	1.000
7	Montgomery County, Kentucky	Powell County, Kentucky	1.000
8	Pike County, Kentucky	Buchanan County, Virginia	1.000
9	Attala County, Mississippi	Madison County, Mississippi	1.000
10	Hinds County, Mississippi	Madison County, Mississippi	1.000
11	Holmes County, Mississippi	Madison County, Mississippi	1.000
12	Leake County, Mississippi	Madison County, Mississippi	1.000
13	Lee County, Mississippi	Union County, Mississippi	1.000
14	Madison County, Mississippi	Rankin County, Mississippi	1.000
15	Madison County, Mississippi	Scott County, Mississippi	1.000
16	Madison County, Mississippi	Yazoo County, Mississippi	1.000
17	Pierce County, North Dakota	Rolette County, North Dakota	1.000
18	Guernsey County, Ohio	Noble County, Ohio	1.000
19	Muskingum County, Ohio	Noble County, Ohio	1.000
20	Noble County, Ohio	Washington County, Ohio	1.000
21	Chattahoochee County, Georgia	Marion County, Georgia	1.000
22	McCreary County, Kentucky	Wayne County, Kentucky	1.000
23	Menifee County, Kentucky	Powell County, Kentucky	1.000
24	Anson County, North Carolina	Marlboro County, South Carolina	1.000
25	Caldwell Parish, Louisiana	Franklin Parish, Louisiana	1.000
26	Switzerland County, Indiana	Gallatin County, Kentucky	1.000
27	Carroll County, Kentucky	Gallatin County, Kentucky	1.000
28	Robeson County, North Carolina	Marlboro County, South Carolina	1.000
29	Gallatin County, Kentucky	Owen County, Kentucky	1.000
30	Clay County, Kentucky	Perry County, Kentucky	1.000
31	Jackson County, Kentucky	Owsley County, Kentucky	1.000
32	Jeff Davis County, Georgia	Wheeler County, Georgia	1.000
33	Martin County, Kentucky	Wayne County, West Virginia	1.000
34	Bottineau County, North Dakota	Rolette County, North Dakota	1.000

35	Coshocton County, Ohio	Holmes County, Ohio	1.000
36	Lampasas County, Texas	San Saba County, Texas	1.000
37	Lee County, Mississippi	Pontotoc County, Mississippi	1.000
38	Frederick County, Virginia	Hardy County, West Virginia	1.000
39	Boone County, West Virginia	Raleigh County, West Virginia	1.000
40	Cumberland County, Tennessee	Fentress County, Tennessee	1.000
41	Buchanan County, Virginia	Mingo County, West Virginia	1.000
42	Rolette County, North Dakota	Towner County, North Dakota	0.999
43	Letcher County, Kentucky	Dickenson County, Virginia	0.999
44	Allen Parish, Louisiana	Vernon Parish, Louisiana	0.999
45	Madison County, Missouri	Perry County, Missouri	0.999
46	Bell County, Kentucky	Leslie County, Kentucky	0.999
47	Laurel County, Kentucky	McCreary County, Kentucky	0.999
48	Holmes County, Ohio	Knox County, Ohio	0.999
49	Johnson County, Kentucky	Morgan County, Kentucky	0.999
50	Pickett County, Tennessee	Scott County, Tennessee	0.999
51	Boyd County, Kentucky	Lawrence County, Kentucky	0.999
52	Richmond County, North Carolina	Marlboro County, South Carolina	0.999
53	Fulton County, Kentucky	Hickman County, Kentucky	0.999
54	Choctaw County, Mississippi	Webster County, Mississippi	0.999
55	Anderson County, Tennessee	Scott County, Tennessee	0.999
56	Issaquena County, Mississippi	Washington County, Mississippi	0.999
57	Gallatin County, Kentucky	Grant County, Kentucky	0.999
58	Hardin County, Illinois	Pope County, Illinois	0.999
59	Lincoln County, Tennessee	Moore County, Tennessee	0.999
60	Lampasas County, Texas	Mills County, Texas	0.998
61	Apache County, Arizona	Greenlee County, Arizona	0.998
62	Gilmer County, Georgia	Murray County, Georgia	0.998
63	Chesterfield County, South Carolina	Marlboro County, South Carolina	0.998
64	Dooly County, Georgia	Houston County, Georgia	0.998
65	Coffee County, Tennessee	Moore County, Tennessee	0.998
66	Chattahoochee County, Georgia	Webster County, Georgia	0.998
67	Clay County, Kentucky	Owsley County, Kentucky	0.998
68	Pendleton County, West Virginia	Pocahontas County, West Virginia	0.998
69	Florence County, South Carolina	Marlboro County, South Carolina	0.998
70	Bryan County, Georgia	Chatham County, Georgia	0.998
71	Knott County, Kentucky	Perry County, Kentucky	0.998
72	McCreary County, Kentucky	Pulaski County, Kentucky	0.998

73	Harlan County, Kentucky	Wise County, Virginia	0.998
74	Carter County, Missouri	Oregon County, Missouri	0.998
75	Caldwell Parish, Louisiana	Ouachita Parish, Louisiana	0.997
76	Monroe County, Ohio	Noble County, Ohio	0.997
77	East Carroll Parish, Louisiana	Issaquena County, Mississippi	0.997
78	Issaquena County, Mississippi	Sharkey County, Mississippi	0.997
79	Morgan County, Ohio	Noble County, Ohio	0.997
80	Morgan County, Tennessee	Scott County, Tennessee	0.997
81	Morgan County, Kentucky	Wolfe County, Kentucky	0.997
82	Jefferson County, Indiana	Scott County, Indiana	0.997
83	Ashland County, Ohio	Holmes County, Ohio	0.997
84	Anderson County, Texas	Cherokee County, Texas	0.997
85	Clark County, Indiana	Scott County, Indiana	0.997
86	Boone County, West Virginia	Kanawha County, West Virginia	0.997
87	Camden County, Missouri	Pulaski County, Missouri	0.997
88	Posey County, Indiana	Union County, Kentucky	0.997
89	La Paz County, Arizona	San Bernardino County, California	0.997
90	Haakon County, South Dakota	Ziebach County, South Dakota	0.997
91	Wayne County, Kentucky	Scott County, Tennessee	0.996
92	Sheridan County, Montana	Divide County, North Dakota	0.996
93	Craighead County, Arkansas	Poinsett County, Arkansas	0.996
94	Marion County, Florida	Sumter County, Florida	0.996
95	Lee County, Mississippi	Prentiss County, Mississippi	0.996
96	Scott County, Indiana	Washington County, Indiana	0.996
97	Bienville Parish, Louisiana	Red River Parish, Louisiana	0.996
98	Grand County, Utah	San Juan County, Utah	0.996
99	Belmont County, Ohio	Noble County, Ohio	0.995
100	Cherokee County, North Carolina	Polk County, Tennessee	0.995
101	Gallatin County, Illinois	Posey County, Indiana	0.995
102	Meriwether County, Georgia	Pike County, Georgia	0.995
103	Union County, Illinois	Perry County, Missouri	0.995
104	Carter County, Missouri	Reynolds County, Missouri	0.995
105	Benson County, North Dakota	Nelson County, North Dakota	0.995
106	Harlan County, Kentucky	Lee County, Virginia	0.995
107	Breathitt County, Kentucky	Magoffin County, Kentucky	0.995
108	Bullitt County, Kentucky	Hardin County, Kentucky	0.995
109	Pike County, Kentucky	Dickenson County, Virginia	0.995
110	Alexander County, Illinois	Cape Girardeau County, Missouri	0.995

111	Reynolds County, Missouri	Wayne County, Missouri	0.995
112	Estill County, Kentucky	Powell County, Kentucky	0.994
113	Lee County, Mississippi	Monroe County, Mississippi	0.994
114	Chicot County, Arkansas	Issaquena County, Mississippi	0.994
115	Clearwater County, Idaho	Shoshone County, Idaho	0.994
116	Plaquemines Parish, Louisiana	Saint Bernard Parish, Louisiana	0.994
117	Perry County, Missouri	Saint Francois County, Missouri	0.994
118	Scotland County, North Carolina	Marlboro County, South Carolina	0.994
119	Macon County, Georgia	Peach County, Georgia	0.994
120	Jeff Davis County, Georgia	Telfair County, Georgia	0.994
121	East Feliciana Parish, Louisiana	Amite County, Mississippi	0.994
122	Clinch County, Georgia	Echols County, Georgia	0.994
123	Bienville Parish, Louisiana	Claiborne Parish, Louisiana	0.994
124	Anderson County, Texas	Freestone County, Texas	0.994
125	Effingham County, Georgia	Jasper County, South Carolina	0.994
126	Arkansas County, Arkansas	Lincoln County, Arkansas	0.994
127	Jefferson County, Alabama	Walker County, Alabama	0.994
128	Magoffin County, Kentucky	Morgan County, Kentucky	0.994
129	Jackson County, Kentucky	Lee County, Kentucky	0.994
130	Lawrence County, Kentucky	Wayne County, West Virginia	0.994
131	Fannin County, Georgia	Polk County, Tennessee	0.993
132	Benton County, Missouri	Camden County, Missouri	0.993
133	Sumner County, Tennessee	Trousdale County, Tennessee	0.993
134	Burnet County, Texas	Lampasas County, Texas	0.993
135	Union County, Arkansas	Claiborne Parish, Louisiana	0.993
136	Jackson County, Indiana	Scott County, Indiana	0.993
137	Chickasaw County, Mississippi	Lee County, Mississippi	0.993
138	Anderson County, Texas	Houston County, Texas	0.993
139	Hickman County, Tennessee	Williamson County, Tennessee	0.992
140	Flagler County, Florida	Putnam County, Florida	0.992
141	Bleckley County, Georgia	Pulaski County, Georgia	0.992
142	Elliott County, Kentucky	Lawrence County, Kentucky	0.992
143	Blount County, Alabama	Walker County, Alabama	0.992
144	Coconino County, Arizona	Mohave County, Arizona	0.992
145	Pulaski County, Missouri	Texas County, Missouri	0.992
146	Burt County, Nebraska	Cuming County, Nebraska	0.992
147	La Paz County, Arizona	Mohave County, Arizona	0.992
148	Glades County, Florida	Okeechobee County, Florida	0.992

149	Franklin County, Illinois	Perry County, Illinois	0.992
150	Sierra County, California	Yuba County, California	0.991
151	McCreary County, Kentucky	Campbell County, Tennessee	0.991
152	Apache County, Arizona	Montezuma County, Colorado	0.991
153	Peach County, Georgia	Taylor County, Georgia	0.991
154	Bedford County, Tennessee	Moore County, Tennessee	0.991
155	Dooly County, Georgia	Sumter County, Georgia	0.991
156	Citrus County, Florida	Sumter County, Florida	0.991
157	Letcher County, Kentucky	Perry County, Kentucky	0.990
158	Cleburne County, Alabama	Randolph County, Alabama	0.990
159	Clay County, Kentucky	Leslie County, Kentucky	0.990
160	Breathitt County, Kentucky	Wolfe County, Kentucky	0.990
161	Haywood County, North Carolina	Cocke County, Tennessee	0.990
162	Issaquena County, Mississippi	Yazoo County, Mississippi	0.990
163	Montgomery County, Georgia	Wheeler County, Georgia	0.990
164	Bradley County, Tennessee	Polk County, Tennessee	0.990
165	Mesa County, Colorado	San Juan County, Utah	0.989
166	Randolph County, West Virginia	Webster County, West Virginia	0.989
167	Hernando County, Florida	Sumter County, Florida	0.989
168	Dewey County, Oklahoma	Major County, Oklahoma	0.989
169	Iron County, Missouri	Reynolds County, Missouri	0.989
170	Breathitt County, Kentucky	Knott County, Kentucky	0.989
171	Dewey County, South Dakota	Ziebach County, South Dakota	0.989
172	Bell County, Kentucky	Harlan County, Kentucky	0.989
173	Pasco County, Florida	Sumter County, Florida	0.989
174	Dade County, Georgia	Hamilton County, Tennessee	0.989
175	Grenada County, Mississippi	Montgomery County, Mississippi	0.989
176	La Paz County, Arizona	Riverside County, California	0.989
177	Dubois County, Indiana	Orange County, Indiana	0.989
178	Cedar County, Nebraska	Clay County, South Dakota	0.988
179	Apache County, Arizona	Graham County, Arizona	0.988
180	Franklin County, Kentucky	Shelby County, Kentucky	0.988
181	Lincoln County, West Virginia	Putnam County, West Virginia	0.988
182	Clinton County, Missouri	DeKalb County, Missouri	0.987
183	Chase County, Kansas	Marion County, Kansas	0.987
184	Carroll County, Mississippi	Grenada County, Mississippi	0.987
185	Desha County, Arkansas	Coahoma County, Mississippi	0.986
186	Ben Hill County, Georgia	Wilcox County, Georgia	0.986

187	Gilmer County, Georgia	Gordon County, Georgia	0.986
188	Mingo County, West Virginia	Wayne County, West Virginia	0.986
189	Spencer County, Indiana	Daviess County, Kentucky	0.986
190	Laurel County, Kentucky	Whitley County, Kentucky	0.985
191	Hardin County, Illinois	Livingston County, Kentucky	0.985
192	Bullock County, Alabama	Russell County, Alabama	0.985
193	Baker County, Georgia	Decatur County, Georgia	0.985
194	Dent County, Missouri	Iron County, Missouri	0.985
195	Bent County, Colorado	Prowers County, Colorado	0.984
196	Darlington County, South Carolina	Marlboro County, South Carolina	0.984
197	Meade County, South Dakota	Ziebach County, South Dakota	0.984
198	Clark County, Kentucky	Estill County, Kentucky	0.984
199	Harrison County, Iowa	Shelby County, Iowa	0.984
200	Brown County, Illinois	Cass County, Illinois	0.984
201	Dooly County, Georgia	Macon County, Georgia	0.984
202	Franklin County, Tennessee	Moore County, Tennessee	0.984
203	Alcorn County, Mississippi	Tippah County, Mississippi	0.983
204	Allen Parish, Louisiana	Beauregard Parish, Louisiana	0.983
205	Cheatham County, Tennessee	Williamson County, Tennessee	0.983
206	Caldwell Parish, Louisiana	Richland Parish, Louisiana	0.983
207	Davis County, Iowa	Monroe County, Iowa	0.983
208	Shenandoah County, Virginia	Hardy County, West Virginia	0.983
209	Tallahatchie County, Mississippi	Yalobusha County, Mississippi	0.982
210	Marion County, Kentucky	Washington County, Kentucky	0.982
211	Pottawattamie County, Iowa	Shelby County, Iowa	0.982
212	Desha County, Arkansas	Phillips County, Arkansas	0.981
213	Dyer County, Tennessee	Lake County, Tennessee	0.981
214	Holmes County, Ohio	Wayne County, Ohio	0.980
215	Chambers County, Alabama	Randolph County, Alabama	0.980
216	Banks County, Georgia	Jackson County, Georgia	0.979
217	Richmond County, Georgia	Edgefield County, South Carolina	0.979
218	Grainger County, Tennessee	Jefferson County, Tennessee	0.979
219	Live Oak County, Texas	San Patricio County, Texas	0.979
220	Levy County, Florida	Marion County, Florida	0.978
221	Jefferson County, Texas	Liberty County, Texas	0.978
222	Crawford County, Iowa	Harrison County, Iowa	0.977
223	Clay County, Kansas	Geary County, Kansas	0.977
224	Adams County, Wisconsin	Wood County, Wisconsin	0.977

225	Adams County, Indiana	Jay County, Indiana	0.977
226	Tuscaloosa County, Alabama	Walker County, Alabama	0.977
227	Coffee County, Georgia	Jeff Davis County, Georgia	0.977
228	Kemper County, Mississippi	Newton County, Mississippi	0.977
229	Nemaha County, Kansas	Pottawatomie County, Kansas	0.977
230	Hamilton County, Texas	Lampasas County, Texas	0.976
231	Carter County, Montana	Custer County, Montana	0.976
232	Bracken County, Kentucky	Harrison County, Kentucky	0.976
233	Mercer County, Kentucky	Washington County, Kentucky	0.976
234	Citrus County, Florida	Levy County, Florida	0.976
235	Sheridan County, Montana	Williams County, North Dakota	0.975
236	Dillon County, South Carolina	Marlboro County, South Carolina	0.975
237	Barbour County, Alabama	Bullock County, Alabama	0.975
238	McDuffie County, Georgia	Taliaferro County, Georgia	0.975
239	Craighead County, Arkansas	Dunklin County, Missouri	0.975
240	Grant County, Indiana	Wells County, Indiana	0.975
241	Jennings County, Indiana	Scott County, Indiana	0.975
242	Bee County, Texas	Refugio County, Texas	0.975
243	Bacon County, Georgia	Coffee County, Georgia	0.975
244	McKinley County, New Mexico	Sandoval County, New Mexico	0.974
245	Crowley County, Colorado	Kiowa County, Colorado	0.974
246	Leake County, Mississippi	Neshoba County, Mississippi	0.974
247	Hickman County, Kentucky	Mississippi County, Missouri	0.973
248	Allen Parish, Louisiana	Jefferson Davis Parish, Louisiana	0.973
249	LaGrange County, Indiana	Saint Joseph County, Michigan	0.973
250	Comanche County, Kansas	Woods County, Oklahoma	0.973
251	Franklin County, Tennessee	Marion County, Tennessee	0.972
252	Trousdale County, Tennessee	Wilson County, Tennessee	0.972
253	Chester County, Tennessee	McNairy County, Tennessee	0.972
254	Nye County, Nevada	White Pine County, Nevada	0.971
255	Pope County, Illinois	Saline County, Illinois	0.971
256	Wibaux County, Montana	Golden Valley County, North Dakota	0.971
257	Caldwell Parish, Louisiana	Catahoula Parish, Louisiana	0.971
258	Macon County, Tennessee	Sumner County, Tennessee	0.970
259	Baker County, Florida	Charlton County, Georgia	0.970
260	Marion County, Georgia	Talbot County, Georgia	0.970
261	Charles County, Maryland	Prince George's County, Maryland	0.970
262	Camas County, Idaho	Elmore County, Idaho	0.969

263	Powell County, Kentucky	Wolfe County, Kentucky	0.969
264	Columbia County, Arkansas	Claiborne Parish, Louisiana	0.969
265	Loving County, Texas	Reeves County, Texas	0.969
266	Greene County, Arkansas	Dunklin County, Missouri	0.969
267	Crawford County, Indiana	Dubois County, Indiana	0.969
268	Russell County, Virginia	Wise County, Virginia	0.969
269	Bullock County, Alabama	Pike County, Alabama	0.969
270	Fallon County, Montana	Golden Valley County, North Dakota	0.968
271	Frederick County, Virginia	Hampshire County, West Virginia	0.968
272	Walker County, Georgia	Hamilton County, Tennessee	0.968
273	Clinch County, Georgia	Ware County, Georgia	0.968
274	Dooly County, Georgia	Wilcox County, Georgia	0.968
275	White County, Illinois	Gibson County, Indiana	0.968
276	Jackson County, Alabama	Franklin County, Tennessee	0.967
277	Angelina County, Texas	Polk County, Texas	0.967
278	Corson County, South Dakota	Dewey County, South Dakota	0.967
279	Cullman County, Alabama	Walker County, Alabama	0.967
280	Gloucester County, Virginia	Mathews County, Virginia	0.966
281	Calhoun County, Mississippi	Yalobusha County, Mississippi	0.966
282	Cassia County, Idaho	Elko County, Nevada	0.966
283	Alachua County, Florida	Marion County, Florida	0.966
284	Houston County, Georgia	Peach County, Georgia	0.966
285	Crisp County, Georgia	Dooly County, Georgia	0.966
286	Athens County, Ohio	Morgan County, Ohio	0.966
287	Douglas County, Missouri	Howell County, Missouri	0.965
288	Bee County, Texas	San Patricio County, Texas	0.965
289	Carter County, Kentucky	Lawrence County, Kentucky	0.965
290	Green County, Kentucky	Hart County, Kentucky	0.965
291	Liberty County, Montana	Pondera County, Montana	0.964
292	Estill County, Kentucky	Lee County, Kentucky	0.964
293	Nevada County, California	Yuba County, California	0.964
294	Guernsey County, Ohio	Tuscarawas County, Ohio	0.964
295	Dodge County, Georgia	Pulaski County, Georgia	0.964
296	Butts County, Georgia	Monroe County, Georgia	0.964
297	Butler County, Kansas	Marion County, Kansas	0.963
298	Clay County, Mississippi	Webster County, Mississippi	0.963
299	Madison County, North Carolina	Cocke County, Tennessee	0.963
300	Montgomery County, Mississippi	Webster County, Mississippi	0.963

301	Crockett County, Tennessee	Dyer County, Tennessee	0.963
302	Bledsoe County, Tennessee	Rhea County, Tennessee	0.962
303	Carroll County, Tennessee	Madison County, Tennessee	0.962
304	Menominee County, Wisconsin	Shawano County, Wisconsin	0.962
305	Van Buren County, Tennessee	Warren County, Tennessee	0.962
306	Roger Mills County, Oklahoma	Wheeler County, Texas	0.961
307	Jackson County, Arkansas	Poinsett County, Arkansas	0.961
308	Catoosa County, Georgia	Walker County, Georgia	0.961
309	Cecil County, Maryland	Lancaster County, Pennsylvania	0.961
310	Montgomery County, Arkansas	Yell County, Arkansas	0.960
311	Lee County, Arkansas	Monroe County, Arkansas	0.960
312	Fallon County, Montana	Slope County, North Dakota	0.960
313	Howard County, Arkansas	Montgomery County, Arkansas	0.960
314	Putnam County, Florida	Volusia County, Florida	0.960
315	Lake County, Tennessee	Obion County, Tennessee	0.960
316	Chester County, Tennessee	Henderson County, Tennessee	0.959
317	Bryan County, Georgia	Evans County, Georgia	0.959
318	Crockett County, Tennessee	Gibson County, Tennessee	0.959
319	Barry County, Missouri	McDonald County, Missouri	0.958
320	Bastrop County, Texas	Fayette County, Texas	0.958
321	Boyle County, Kentucky	Washington County, Kentucky	0.958
322	Crawford County, Missouri	Iron County, Missouri	0.958
323	Jefferson County, Montana	Madison County, Montana	0.958
324	Fannin County, Georgia	Murray County, Georgia	0.958
325	Preston County, West Virginia	Taylor County, West Virginia	0.957
326	Madison County, North Carolina	Greene County, Tennessee	0.957
327	Drew County, Arkansas	Lincoln County, Arkansas	0.957
328	Union County, Illinois	Cape Girardeau County, Missouri	0.957
329	Clay County, Georgia	Quitman County, Georgia	0.957
330	Cape Girardeau County, Missouri	Scott County, Missouri	0.957
331	Clinton County, Pennsylvania	Union County, Pennsylvania	0.957
332	McDowell County, West Virginia	Mercer County, West Virginia	0.957
333	Franklin County, Alabama	Marion County, Alabama	0.956
334	Kootenai County, Idaho	Shoshone County, Idaho	0.956
335	LaGrange County, Indiana	Noble County, Indiana	0.956
336	Polk County, Texas	Tyler County, Texas	0.956
337	Letcher County, Kentucky	Wise County, Virginia	0.956
338	Lawrence County, Kentucky	Morgan County, Kentucky	0.956

339	Decatur County, Indiana	Jennings County, Indiana	0.956
340	Hamilton County, Tennessee	Marion County, Tennessee	0.955
341	Van Buren County, Tennessee	White County, Tennessee	0.955
342	Lafayette County, Arkansas	Caddo Parish, Louisiana	0.955
343	Jackson County, Georgia	Oconee County, Georgia	0.955
344	Holmes County, Ohio	Tuscarawas County, Ohio	0.955
345	Claiborne Parish, Louisiana	Webster Parish, Louisiana	0.955
346	Monroe County, Arkansas	Saint Francis County, Arkansas	0.955
347	Harris County, Texas	Liberty County, Texas	0.955
348	Page County, Virginia	Warren County, Virginia	0.955
349	Daniels County, Montana	Valley County, Montana	0.955
350	Marion County, Alabama	Walker County, Alabama	0.954
351	Crawford County, Georgia	Peach County, Georgia	0.954
352	Garrard County, Kentucky	Rockcastle County, Kentucky	0.954
353	Grenada County, Mississippi	Tallahatchie County, Mississippi	0.954
354	Paulding County, Georgia	Polk County, Georgia	0.953
355	Blaine County, Idaho	Elmore County, Idaho	0.953
356	Houston County, Georgia	Pulaski County, Georgia	0.953
357	Brown County, Indiana	Jackson County, Indiana	0.953
358	Cabell County, West Virginia	Lincoln County, West Virginia	0.953
359	Marshall County, Kansas	Pottawatomie County, Kansas	0.953
360	Banks County, Georgia	Madison County, Georgia	0.953
361	Claiborne County, Tennessee	Hancock County, Tennessee	0.953
362	Jefferson County, Oregon	Linn County, Oregon	0.953
363	Lee County, Virginia	Scott County, Virginia	0.952
364	Hardin County, Illinois	Crittenden County, Kentucky	0.952
365	Chattahoochee County, Georgia	Muscogee County, Georgia	0.952
366	Grant County, West Virginia	Mineral County, West Virginia	0.952
367	Bryan County, Georgia	Bulloch County, Georgia	0.952
368	Buchanan County, Missouri	DeKalb County, Missouri	0.952
369	Delaware County, Oklahoma	Ottawa County, Oklahoma	0.951
370	Carroll County, Mississippi	Holmes County, Mississippi	0.951
371	Grant County, Kentucky	Harrison County, Kentucky	0.951
372	Shoshone County, Idaho	Sanders County, Montana	0.950
373	Duplin County, North Carolina	Onslow County, North Carolina	0.950
374	Cibola County, New Mexico	McKinley County, New Mexico	0.950
375	Coleman County, Texas	Concho County, Texas	0.950
376	Adair County, Kentucky	Casey County, Kentucky	0.950

377	Lincoln County, Nevada	Millard County, Utah	0.950
378	Atoka County, Oklahoma	Choctaw County, Oklahoma	0.949
379	Coahoma County, Mississippi	Tallahatchie County, Mississippi	0.949
380	Winnebago County, Illinois	Green County, Wisconsin	0.949
381	Clay County, West Virginia	Roane County, West Virginia	0.949
382	Callahan County, Texas	Jones County, Texas	0.949
383	Boundary County, Idaho	Lincoln County, Montana	0.949
384	Attala County, Mississippi	Choctaw County, Mississippi	0.949
385	Mono County, California	Lyon County, Nevada	0.949
386	Menifee County, Kentucky	Wolfe County, Kentucky	0.948
387	Atoka County, Oklahoma	Pushmataha County, Oklahoma	0.948
388	Worcester County, Maryland	Accomack County, Virginia	0.948
389	Juniata County, Pennsylvania	Perry County, Pennsylvania	0.948
390	Latah County, Idaho	Shoshone County, Idaho	0.948
391	Briscoe County, Texas	Donley County, Texas	0.947
392	Adams County, Ohio	Highland County, Ohio	0.947
393	Toombs County, Georgia	Treutlen County, Georgia	0.947
394	Lafayette County, Mississippi	Union County, Mississippi	0.947
395	Barbour County, West Virginia	Harrison County, West Virginia	0.947
396	Orleans Parish, Louisiana	Saint Bernard Parish, Louisiana	0.947
397	Highlands County, Florida	Okeechobee County, Florida	0.947
398	Jackson County, Illinois	Randolph County, Illinois	0.947
399	Bonner County, Idaho	Shoshone County, Idaho	0.946
400	Mesa County, Colorado	Pitkin County, Colorado	0.946
401	Fayette County, Tennessee	Tipton County, Tennessee	0.946
402	Montrose County, Colorado	San Juan County, Utah	0.946
403	Wayne County, Indiana	Darke County, Ohio	0.946
404	Cleveland County, Arkansas	Lincoln County, Arkansas	0.946
405	Bowman County, North Dakota	Slope County, North Dakota	0.946
406	McIntosh County, Georgia	Wayne County, Georgia	0.946
407	Buchanan County, Virginia	McDowell County, West Virginia	0.945
408	Hickman County, Kentucky	Obion County, Tennessee	0.945
409	Sioux County, Nebraska	Fall River County, South Dakota	0.945
410	Meriwether County, Georgia	Talbot County, Georgia	0.944
411	Rapides Parish, Louisiana	Vernon Parish, Louisiana	0.944
412	Franklin County, Missouri	Washington County, Missouri	0.944
413	Raleigh County, West Virginia	Wyoming County, West Virginia	0.944
414	Barrow County, Georgia	Gwinnett County, Georgia	0.944

415	Adams County, Indiana	Allen County, Indiana	0.944
416	Clay County, Kentucky	Laurel County, Kentucky	0.944
417	Benton County, Missouri	Hickory County, Missouri	0.944
418	Lake County, Florida	Sumter County, Florida	0.944
419	Benson County, North Dakota	Towner County, North Dakota	0.944
420	Scott County, Virginia	Wise County, Virginia	0.944
421	Dillon County, South Carolina	Horry County, South Carolina	0.944
422	Kanawha County, West Virginia	Lincoln County, West Virginia	0.943
423	Henry County, Kentucky	Shelby County, Kentucky	0.943
424	Howell County, Missouri	Texas County, Missouri	0.943
425	Eddy County, New Mexico	Loving County, Texas	0.943
426	Crittenden County, Arkansas	Shelby County, Tennessee	0.942
427	Murray County, Georgia	Bradley County, Tennessee	0.942
428	Ben Hill County, Georgia	Turner County, Georgia	0.942
429	Churchill County, Nevada	Pershing County, Nevada	0.941
430	Leake County, Mississippi	Winston County, Mississippi	0.941
431	Bollinger County, Missouri	Madison County, Missouri	0.941
432	Brown County, Illinois	Schuyler County, Illinois	0.941
433	Grant County, West Virginia	Randolph County, West Virginia	0.941
434	Oldham County, Kentucky	Trimble County, Kentucky	0.941
435	Fentress County, Tennessee	Pickett County, Tennessee	0.941
436	DeKalb County, Alabama	Dade County, Georgia	0.940
437	Bledsoe County, Tennessee	White County, Tennessee	0.940
438	Liberty County, Georgia	McIntosh County, Georgia	0.940
439	Cooper County, Missouri	Pettis County, Missouri	0.940
440	Sioux County, Iowa	Union County, South Dakota	0.940
441	Chattahoochee County, Georgia	Talbot County, Georgia	0.939
442	Monroe County, Illinois	Jefferson County, Missouri	0.939
443	Appanoose County, Iowa	Monroe County, Iowa	0.939
444	Wallowa County, Oregon	Columbia County, Washington	0.939
445	Long County, Georgia	McIntosh County, Georgia	0.939
446	Rusk County, Wisconsin	Taylor County, Wisconsin	0.938
447	Grant Parish, Louisiana	Rapides Parish, Louisiana	0.938
448	Henderson County, Kentucky	McLean County, Kentucky	0.938
449	Dewey County, Oklahoma	Woodward County, Oklahoma	0.938
450	Big Horn County, Montana	Treasure County, Montana	0.938
451	Elk County, Kansas	Wilson County, Kansas	0.938
452	Caldwell Parish, Louisiana	Winn Parish, Louisiana	0.938

453	Monroe County, Tennessee	Polk County, Tennessee	0.938
454	Hartley County, Texas	Sherman County, Texas	0.937
455	Monroe County, Iowa	Wayne County, Iowa	0.937
456	Grant County, West Virginia	Hampshire County, West Virginia	0.937
457	Cass County, Missouri	Henry County, Missouri	0.937
458	Overton County, Tennessee	Pickett County, Tennessee	0.937
459	Oktibbeha County, Mississippi	Webster County, Mississippi	0.936
460	Laclede County, Missouri	Pulaski County, Missouri	0.936
461	Pennington County, South Dakota	Ziebach County, South Dakota	0.936
462	Liberty County, Montana	Toole County, Montana	0.936
463	Gallatin County, Montana	Jefferson County, Montana	0.936
464	Bland County, Virginia	Smyth County, Virginia	0.935
465	Caldwell County, Missouri	DeKalb County, Missouri	0.935
466	Sequatchie County, Tennessee	Van Buren County, Tennessee	0.935
467	Price County, Wisconsin	Taylor County, Wisconsin	0.935
468	Shannon County, Missouri	Texas County, Missouri	0.934
469	Richmond County, Virginia	Westmoreland County, Virginia	0.934
470	Pope County, Arkansas	Van Buren County, Arkansas	0.934
471	Surry County, North Carolina	Patrick County, Virginia	0.933
472	Miller County, Missouri	Osage County, Missouri	0.933
473	Jones County, Texas	Shackelford County, Texas	0.933
474	George County, Mississippi	Greene County, Mississippi	0.933
475	Fleming County, Kentucky	Mason County, Kentucky	0.932
476	Delaware County, Iowa	Dubuque County, Iowa	0.932
477	Garrard County, Kentucky	Lincoln County, Kentucky	0.932
478	Cumberland County, Tennessee	Putnam County, Tennessee	0.932
479	Hall County, Georgia	Jackson County, Georgia	0.932
480	Custer County, Montana	Garfield County, Montana	0.932
481	Spencer County, Indiana	Hancock County, Kentucky	0.931
482	Issaquena County, Mississippi	Warren County, Mississippi	0.931
483	Roosevelt County, Montana	Sheridan County, Montana	0.931
484	Green County, Kentucky	Metcalfe County, Kentucky	0.931
485	Bracken County, Kentucky	Clermont County, Ohio	0.930
486	Norton County, Kansas	Red Willow County, Nebraska	0.930
487	Hidalgo County, Texas	Kenedy County, Texas	0.930
488	Gilmer County, West Virginia	Lewis County, West Virginia	0.929
489	Choctaw County, Alabama	Marengo County, Alabama	0.929
490	Collier County, Florida	Monroe County, Florida	0.929

491	Ben Hill County, Georgia	Telfair County, Georgia	0.929
492	Hartley County, Texas	Potter County, Texas	0.928
493	Claiborne County, Tennessee	Grainger County, Tennessee	0.928
494	Pike County, Georgia	Upson County, Georgia	0.928
495	Montgomery County, North Carolina	Richmond County, North Carolina	0.928
496	Fayette County, West Virginia	Summers County, West Virginia	0.928
497	Jefferson County, Arkansas	Lincoln County, Arkansas	0.928
498	Hickman County, Tennessee	Maury County, Tennessee	0.928
499	Grays Harbor County, Washington	Jefferson County, Washington	0.928
500	Anne Arundel County, Maryland	Prince George's County, Maryland	0.927
501	Irion County, Texas	Tom Green County, Texas	0.927
502	Catron County, New Mexico	Sierra County, New Mexico	0.927
503	Cumberland County, Tennessee	Morgan County, Tennessee	0.927
504	Pendleton County, West Virginia	Randolph County, West Virginia	0.927
505	Bollinger County, Missouri	Wayne County, Missouri	0.926
506	Bryan County, Georgia	Liberty County, Georgia	0.926
507	La Paz County, Arizona	Imperial County, California	0.926
508	Carson County, Texas	Donley County, Texas	0.926
509	Emanuel County, Georgia	Johnson County, Georgia	0.926
510	Claiborne County, Tennessee	Union County, Tennessee	0.926
511	Anderson County, Tennessee	Campbell County, Tennessee	0.925
512	Benson County, North Dakota	Eddy County, North Dakota	0.925
513	Anderson County, Texas	Henderson County, Texas	0.925
514	Adams County, Wisconsin	Portage County, Wisconsin	0.925
515	Floyd County, Virginia	Pulaski County, Virginia	0.925
516	Lee County, Arkansas	Phillips County, Arkansas	0.925
517	Richland County, Montana	McKenzie County, North Dakota	0.925
518	Alleghany County, Virginia	Botetourt County, Virginia	0.925
519	Jackson County, Kansas	Nemaha County, Kansas	0.924
520	Harrison County, Kentucky	Nicholas County, Kentucky	0.924
521	Clarke County, Alabama	Wilcox County, Alabama	0.924
522	Baker County, Georgia	Miller County, Georgia	0.924
523	Brown County, South Dakota	McPherson County, South Dakota	0.924
524	Douglas County, Colorado	Teller County, Colorado	0.924
525	Hamblen County, Tennessee	Jefferson County, Tennessee	0.924
526	Gratiot County, Michigan	Isabella County, Michigan	0.924
527	Bourbon County, Kentucky	Nicholas County, Kentucky	0.924
528	Craig County, Virginia	Giles County, Virginia	0.924

529	Hardeman County, Tennessee	McNairy County, Tennessee	0.924
530	Beaufort County, South Carolina	Colleton County, South Carolina	0.923
531	Calvert County, Maryland	Prince George's County, Maryland	0.923
532	Eastland County, Texas	Erath County, Texas	0.923
533	Franklin County, Illinois	Jefferson County, Illinois	0.923
534	Dale County, Alabama	Houston County, Alabama	0.923
535	Calhoun County, Mississippi	Grenada County, Mississippi	0.922
536	Caroline County, Maryland	Talbot County, Maryland	0.922
537	Logan County, West Virginia	Wyoming County, West Virginia	0.921
538	Maries County, Missouri	Osage County, Missouri	0.921
539	Grant County, West Virginia	Tucker County, West Virginia	0.921
540	Carroll County, Arkansas	Newton County, Arkansas	0.921
541	Macon County, Illinois	Moultrie County, Illinois	0.921
542	Allen Parish, Louisiana	Evangeline Parish, Louisiana	0.921
543	Hart County, Kentucky	Larue County, Kentucky	0.921
544	Dewey County, Oklahoma	Roger Mills County, Oklahoma	0.920
545	Creek County, Oklahoma	Osage County, Oklahoma	0.920
546	Jefferson County, Oregon	Marion County, Oregon	0.920
547	Randolph County, Alabama	Carroll County, Georgia	0.919
548	Carroll County, Missouri	Ray County, Missouri	0.919
549	Cedar County, Iowa	Scott County, Iowa	0.919
550	Baker County, Florida	Nassau County, Florida	0.919
551	DeKalb County, Indiana	LaGrange County, Indiana	0.919
552	Hancock County, Mississippi	Harrison County, Mississippi	0.919
553	Pecos County, Texas	Ward County, Texas	0.919
554	Trinity County, Texas	Walker County, Texas	0.919
555	Lafayette County, Arkansas	Bossier Parish, Louisiana	0.917
556	Owyhee County, Idaho	Humboldt County, Nevada	0.917
557	Lincoln County, Nevada	Nye County, Nevada	0.917
558	Grand County, Colorado	Larimer County, Colorado	0.917
559	Smyth County, Virginia	Wythe County, Virginia	0.917
560	Jasper County, Iowa	Tama County, Iowa	0.917
561	Campbell County, South Dakota	Walworth County, South Dakota	0.916
562	Floyd County, Kentucky	Pike County, Kentucky	0.916
563	Cherokee County, Georgia	Gordon County, Georgia	0.916
564	Marion County, Kentucky	Nelson County, Kentucky	0.915
565	Hill County, Montana	Liberty County, Montana	0.915
566	Bracken County, Kentucky	Pendleton County, Kentucky	0.915

567	Lewis County, New York	Oswego County, New York	0.914
568	Elko County, Nevada	Box Elder County, Utah	0.914
569	Estill County, Kentucky	Madison County, Kentucky	0.914
570	McDonald County, Missouri	Delaware County, Oklahoma	0.914
571	Buchanan County, Iowa	Delaware County, Iowa	0.914
572	Hart County, Georgia	Madison County, Georgia	0.914
573	Desha County, Arkansas	Bolivar County, Mississippi	0.914
574	Lincoln County, Wisconsin	Taylor County, Wisconsin	0.914
575	Kemper County, Mississippi	Lauderdale County, Mississippi	0.913
576	Adams County, Indiana	Van Wert County, Ohio	0.913
577	Boundary County, Idaho	Pend Oreille County, Washington	0.913
578	Baker County, Florida	Duval County, Florida	0.913
579	Dubois County, Indiana	Perry County, Indiana	0.912
580	Kane County, Utah	San Juan County, Utah	0.912
581	Catahoula Parish, Louisiana	Franklin Parish, Louisiana	0.912
582	Douglas County, Missouri	Ozark County, Missouri	0.912
583	Cumberland County, Tennessee	Roane County, Tennessee	0.912
584	Bledsoe County, Tennessee	Sequatchie County, Tennessee	0.911
585	Hampshire County, West Virginia	Morgan County, West Virginia	0.911
586	Daviess County, Missouri	DeKalb County, Missouri	0.911
587	Floyd County, Kentucky	Magoffin County, Kentucky	0.911
588	Crawford County, Kansas	Barton County, Missouri	0.911
589	Henderson County, Tennessee	Madison County, Tennessee	0.911
590	Brown County, Texas	San Saba County, Texas	0.911
591	Greenlee County, Arizona	Catron County, New Mexico	0.911
592	Humboldt County, Nevada	Pershing County, Nevada	0.911
593	Carter County, Missouri	Shannon County, Missouri	0.911
594	Bibb County, Georgia	Peach County, Georgia	0.910
595	Johnson County, Illinois	Saline County, Illinois	0.910
596	Dixon County, Nebraska	Clay County, South Dakota	0.910
597	Christian County, Kentucky	Muhlenberg County, Kentucky	0.910
598	Clark County, Wisconsin	Eau Claire County, Wisconsin	0.910
599	Rankin County, Mississippi	Smith County, Mississippi	0.909
600	Randolph County, West Virginia	Upshur County, West Virginia	0.909
601	Lycoming County, Pennsylvania	Union County, Pennsylvania	0.909
602	Mingo County, West Virginia	Wyoming County, West Virginia	0.909
603	Nueces County, Texas	San Patricio County, Texas	0.908
604	Lassen County, California	Shasta County, California	0.908

605	Quitman County, Georgia	Randolph County, Georgia	0.908
606	Desha County, Arkansas	Lincoln County, Arkansas	0.908
607	Marshall County, Minnesota	Grand Forks County, North Dakota	0.908
608	Oregon County, Missouri	Ripley County, Missouri	0.907
609	Lafayette County, Mississippi	Yalobusha County, Mississippi	0.907
610	Ochiltree County, Texas	Roberts County, Texas	0.907
611	Rockingham County, Virginia	Pendleton County, West Virginia	0.907
612	Grand County, Utah	Wayne County, Utah	0.907
613	Marshall County, Iowa	Tama County, Iowa	0.906
614	Adams County, Wisconsin	Sauk County, Wisconsin	0.906
615	Marion County, Arkansas	Taney County, Missouri	0.906
616	Concho County, Texas	Runnels County, Texas	0.906
617	Lyon County, Iowa	Minnehaha County, South Dakota	0.906
618	Custer County, Colorado	Huerfano County, Colorado	0.906
619	Crowley County, Colorado	El Paso County, Colorado	0.906
620	Phelps County, Missouri	Pulaski County, Missouri	0.906
621	Baker County, Georgia	Calhoun County, Georgia	0.905
622	Newaygo County, Michigan	Oceana County, Michigan	0.905
623	Harlan County, Kentucky	Perry County, Kentucky	0.905
624	Lamar County, Georgia	Monroe County, Georgia	0.905
625	Custer County, Colorado	Pueblo County, Colorado	0.904
626	Fergus County, Montana	Musselshell County, Montana	0.904
627	Bailey County, Texas	Hockley County, Texas	0.904
628	Itawamba County, Mississippi	Prentiss County, Mississippi	0.904
629	Floyd County, Georgia	Polk County, Georgia	0.904
630	Conway County, Arkansas	Pope County, Arkansas	0.903
631	Emanuel County, Georgia	Toombs County, Georgia	0.903
632	Wibaux County, Montana	McKenzie County, North Dakota	0.903
633	Gilmer County, Georgia	Lumpkin County, Georgia	0.903
634	Polk County, Florida	Sumter County, Florida	0.903
635	Clinton County, Illinois	Marion County, Illinois	0.902
636	Grant County, Arkansas	Saline County, Arkansas	0.902
637	Monongalia County, West Virginia	Preston County, West Virginia	0.901
638	Sumter County, Alabama	Kemper County, Mississippi	0.901
639	Gearry County, Kansas	Riley County, Kansas	0.901
640	Cooper County, Missouri	Morgan County, Missouri	0.901
641	Juneau County, Wisconsin	Vernon County, Wisconsin	0.901
642	Essex County, Virginia	Richmond County, Virginia	0.900

643	Hamilton County, Illinois	Saline County, Illinois	0.900
644	Kenedy County, Texas	Willacy County, Texas	0.900
645	Monroe County, Ohio	Tyler County, West Virginia	0.900
646	Jackson Parish, Louisiana	Ouachita Parish, Louisiana	0.900
647	Chaves County, New Mexico	Lincoln County, New Mexico	0.900
648	Cuming County, Nebraska	Dodge County, Nebraska	0.899
649	Davis County, Iowa	Wapello County, Iowa	0.899
650	Carter County, Montana	Butte County, South Dakota	0.899
651	Franklin Parish, Louisiana	Richland Parish, Louisiana	0.899
652	Crittenden County, Arkansas	Lee County, Arkansas	0.898
653	Kemper County, Mississippi	Winston County, Mississippi	0.898
654	Franklin County, Illinois	Jackson County, Illinois	0.897
655	Chambers County, Alabama	Harris County, Georgia	0.897
656	Boone County, West Virginia	Wyoming County, West Virginia	0.897
657	Crane County, Texas	Pecos County, Texas	0.897
658	Berkshire County, Massachusetts	Rensselaer County, New York	0.897
659	Hampton County, South Carolina	Jasper County, South Carolina	0.896
660	Fulton County, Kentucky	Weakley County, Tennessee	0.896
661	Jim Wells County, Texas	San Patricio County, Texas	0.896
662	Chatham County, Georgia	Effingham County, Georgia	0.896
663	Fayette County, Alabama	Walker County, Alabama	0.895
664	Beaver County, Oklahoma	Ellis County, Oklahoma	0.895
665	Camden County, Missouri	Morgan County, Missouri	0.895
666	Franklin County, North Carolina	Warren County, North Carolina	0.895
667	Brazos County, Texas	Leon County, Texas	0.895
668	Idaho County, Idaho	Missoula County, Montana	0.895
669	Cascade County, Montana	Chouteau County, Montana	0.895
670	Jackson County, Colorado	Albany County, Wyoming	0.895
671	Benton County, Arkansas	McDonald County, Missouri	0.894
672	Bacon County, Georgia	Ware County, Georgia	0.894
673	Lake County, Montana	Missoula County, Montana	0.894
674	Montgomery County, Arkansas	Pike County, Arkansas	0.894
675	Franklin County, Indiana	Ripley County, Indiana	0.894
676	Christian County, Illinois	Shelby County, Illinois	0.894
677	Logan County, Colorado	Kimball County, Nebraska	0.894
678	Pickens County, Alabama	Noxubee County, Mississippi	0.894
679	Scott County, Minnesota	Sibley County, Minnesota	0.893
680	Clay County, Minnesota	Richland County, North Dakota	0.893

681	Claiborne Parish, Louisiana	Union Parish, Louisiana	0.893
682	Custer County, Oklahoma	Roger Mills County, Oklahoma	0.893
683	Aurora County, South Dakota	Davison County, South Dakota	0.893
684	Jasper County, Iowa	Poweshiek County, Iowa	0.893
685	Madison County, Georgia	Oglethorpe County, Georgia	0.892
686	Marion County, Florida	Putnam County, Florida	0.892
687	Jackson Parish, Louisiana	Lincoln Parish, Louisiana	0.892
688	Henry County, Missouri	Johnson County, Missouri	0.892
689	Fleming County, Kentucky	Nicholas County, Kentucky	0.892
690	Lee County, Texas	Milam County, Texas	0.891
691	Swain County, North Carolina	Cocke County, Tennessee	0.890
692	Humboldt County, Nevada	Malheur County, Oregon	0.890
693	Calhoun County, South Carolina	Clarendon County, South Carolina	0.890
694	Lucas County, Iowa	Monroe County, Iowa	0.890
695	Emmons County, North Dakota	Morton County, North Dakota	0.890
696	East Feliciana Parish, Louisiana	Saint Helena Parish, Louisiana	0.890
697	Allen Parish, Louisiana	Rapides Parish, Louisiana	0.890
698	Jefferson County, Iowa	Wapello County, Iowa	0.889
699	Treutlen County, Georgia	Wheeler County, Georgia	0.889
700	Bell County, Texas	Williamson County, Texas	0.889
701	Archer County, Texas	Wichita County, Texas	0.889
702	Angelina County, Texas	Trinity County, Texas	0.888
703	Harrison County, Ohio	Tuscarawas County, Ohio	0.888
704	Crockett County, Tennessee	Lauderdale County, Tennessee	0.888
705	Fayette County, Pennsylvania	Somerset County, Pennsylvania	0.888
706	Crittenden County, Arkansas	Saint Francis County, Arkansas	0.887
707	Anderson County, Texas	Leon County, Texas	0.887
708	Muhlenberg County, Kentucky	Todd County, Kentucky	0.887
709	Adair County, Missouri	Schuyler County, Missouri	0.887
710	La Paz County, Arizona	Maricopa County, Arizona	0.886
711	Itawamba County, Mississippi	Monroe County, Mississippi	0.886
712	Cerro Gordo County, Iowa	Mitchell County, Iowa	0.886
713	Sussex County, Delaware	Wicomico County, Maryland	0.886
714	Arkansas County, Arkansas	Monroe County, Arkansas	0.885
715	San Augustine County, Texas	Shelby County, Texas	0.885
716	Boyle County, Kentucky	Lincoln County, Kentucky	0.885
717	Caldwell County, Kentucky	Lyon County, Kentucky	0.885
718	Mason County, Michigan	Oceana County, Michigan	0.885

719	Leon County, Texas	Madison County, Texas	0.885
720	Highland County, Virginia	Pendleton County, West Virginia	0.885
721	Vermillion County, Indiana	Warren County, Indiana	0.884
722	Morgan County, Ohio	Muskingum County, Ohio	0.884
723	Brown County, Illinois	Morgan County, Illinois	0.883
724	Davison County, South Dakota	Douglas County, South Dakota	0.883
725	Cross County, Arkansas	Saint Francis County, Arkansas	0.883
726	Reeves County, Texas	Ward County, Texas	0.883
727	Benton County, Tennessee	Houston County, Tennessee	0.883
728	Placer County, California	Yuba County, California	0.882
729	Chippewa County, Wisconsin	Taylor County, Wisconsin	0.882
730	Whitley County, Kentucky	Campbell County, Tennessee	0.882
731	Marshall County, Iowa	Poweshiek County, Iowa	0.882

TABLE S1. Reported spatial disparities in lung cancer mortality between neighboring US counties.